

# Simulating quantum emitters in arbitrary photonic environments using FDTD: beyond the semi-classical regime

Qingyi Zhou,<sup>1,\*</sup> S. Ali Hassani Gangaraj,<sup>2</sup> Ming Zhou,<sup>3</sup> and Zongfu Yu<sup>1,†</sup>

<sup>1</sup>*Department of Electrical and Computer Engineering,  
University of Wisconsin-Madison, Madison, WI 53706, USA*

<sup>2</sup>*Optical Physics Division, Corning Research and Development Corporation,  
Sullivan Park, Corning, NY 14831, USA*

<sup>3</sup>*Department of Electrical Engineering, Stanford University, Stanford, CA 94305, USA*

(Dated: October 22, 2024)

We propose a numerical algorithm that integrates quantum two-level systems (TLSs) into the finite-difference time-domain (FDTD) framework for simulating quantum emitters in arbitrary 3D photonic environments. Conventional methods struggle with these systems due to their semi-classical nature and spurious self-interactions that arise when a TLS is driven by its own radiation field. We address these issues by determining the correct electric field for driving the TLS, as well as the current source used in FDTD for modeling photon emission. Our method, focusing on single-excitation states, employs a total field-incident field (TF-IF) technique to eliminate self-interactions, enabling precise simulations of photon emission and scattering. The algorithm also successfully models complex phenomena such as resonant energy transfer, superradiance, and vacuum Rabi splitting. This powerful computational tool is expected to substantially advance research in nanophotonics, quantum physics, and beyond.

## I. INTRODUCTION

Classical electrodynamics, governed by Maxwell's equations, has played an important role in understanding and designing electromagnetic devices. This foundational theory has influenced a variety of scientific and technological fields. The most popular method for numerically solving Maxwell's equations is the finite-difference time-domain (FDTD) method [1], with efficient and mature solvers that are widely available [2, 3]. As the frontiers of science push deeper into the quantum realm, advances in quantum physics [4, 5] and chemistry [6–8] are driving the demand for a more profound understanding of light-matter interactions at the quantum level, and the limitations of Maxwell's equations become evident. The dynamics of multiple quantum two-level systems (TLSs) interacting within complex photonic environment [9–17],

challenge existing simulation techniques. While analytical solutions are feasible for simple photonic environments like single-mode optical cavities [18–20] or single-mode waveguides [21, 22], it's difficult to generalize these solutions to arbitrary photonic environment, and researchers still need to rely on numerical techniques.

Currently, the simulation techniques used to tackle this issue can be divided into two categories: semi-classical methods, and approaches based on master equation [23–25]. The semi-classical methods, such as Maxwell-Bloch [26, 27] or Maxwell-Schrödinger equations [28–30], are limited by their reliance on classical fields, and often fail to correctly account for incoherent processes [31]. They also require careful treatment of self-interaction, which is often overlooked in previous works [32, 33]. On the other hand, for master equation approaches the photon degrees of freedom is often traced out. These approaches rely on calculating dyadic Green's functions and become computationally expensive for large number of quantum elements. Moreover, employing the Born-Markov approximation leads to inaccurate results when

---

\* [qzhou75@wisc.edu](mailto:qzhou75@wisc.edu)

† [zyu54@wisc.edu](mailto:zyu54@wisc.edu)

memory effects become important [34–36]. The above issues have made it quite difficult to accurately simulate multiple TLSs in arbitrary environment. Currently, a general algorithm that has been thoroughly tested is still lacking, which hinders research in quantum physics and nanophotonics.

In this paper, we aim to address the above issues and provide a simulation technique that’s available for use. We propose an algorithm based on 3D FDTD due to the fact that FDTD is both versatile and highly efficient. To incorporate quantum two-level systems (TLSs) into FDTD, the problem is first simplified by focusing on single-excitation states. We rigorously analyze the dynamics of TLSs driven by the electric field, as well as how TLSs couple back to Maxwell’s equations through radiation emission. To avoid unwanted self-interaction, which is essential for accurate results, we propose a total field-incident field (TF-IF) technique to exclude the primary radiation field from driving the TLS. We first validate our approach through benchmark examples involving one TLS, demonstrating that our method accurately computes the spontaneous emission rates and scattering cross sections, which is not possible without mitigating self-interaction effects. Further, we extend our simulations to systems involving  $N \geq 2$  TLSs, exploring phenomena such as excitation transport between TLSs, superradiance in TLS arrays, as well as vacuum Rabi splitting when TLSs are strongly coupled to a ring resonator. These examples demonstrate the capability of our proposed algorithm to simulate dynamics of multiple TLSs placed within complex 3D photonic environments, which, to the best of our knowledge, has never been conducted successfully before. The implementation of this algorithm has been realized in CUDA C++, with the code made publicly available on [GitHub](#). Currently, we are working on integrating this algorithm into Tidy3d [2] simulation platform to ensure its availability in the near future, with the hope that it will serve as a valuable tool for researchers across various fields.

## II. METHODOLOGY

The optical properties of hybrid systems that combine quantum emitters (such as atoms or quantum dots) with complex photonic environment are of much current interest. It is possible to derive analytical solution for very simple structures such as single-mode optical cavity [18] or waveguide [21, 22] under certain approximations. However when the problem involves multiple TLSs inside a more complicated environment (for example, a multi-mode cavity [37–40], or photonic crystal [13, 41–45]), simple analytical solution might not be available, and it is necessary to incorporate TLSs into full-wave electromagnetic simulation. Many researchers have been working on this topic, and the most popular methods mainly fall into 2 categories: semi-classical methods [26–30, 32, 33, 46–52], often formulated by combining classical Maxwell’s equations with an extra set of equations that can describe the TLSs’ dynamics; master equation approaches, which rely on tracing out the photon degrees of freedom.

Here, by combining TLSs’ dynamics with FDTD, our proposed method is similar to the semi-classical methods mentioned above. Before introducing the implementation details, we will first answer two vital questions: (1) what is the electric field value that should be used to drive the TLS; (2) what is the source term that should be used in Maxwell’s equations when considering radiation of the TLS. As will be shown later, the answers to these questions are crucial for incorporating TLS dynamics into Maxwell’s equations correctly.

### A. Driving term related to TLS dynamics

To correctly simulate a hybrid system containing both TLSs and photonic environment, it is required to understand how the electromagnetic fields affect the dynamics of TLSs. In this section, without loss of generality, we focus on the dynamics of one TLS. The resonance frequency of the TLS is denoted as  $\omega_0$ , and the corresponding resonance wavelength is rep-

resented by  $\lambda_0$ . Its spontaneous emission rate inside vacuum is denoted as  $\Gamma_{\text{vac}}$ . These notations are consistently used throughout the paper. To make our discussions general, instead of limiting ourselves to a certain set of equations, we use a more generalized notation  $\vec{u}(t)$  to describe the status of TLS. When a TLS is driven by electric field, the governing ordinary equations can be summarized as

$$\frac{d}{dt}\vec{u}(t) = \{\text{Decay term}\} + \{\text{Driving term}\} \quad (1)$$

$$\triangleq \Gamma\mathcal{L}(\vec{u}) + f(\vec{u}) \cdot \vec{E},$$

where  $\Gamma$  denotes the decay rate, and  $\vec{E}$  denotes the electric field value that's used to drive the TLS. Physically, the electric fields inside the simulation domain can be divided into 3 parts:  $\vec{E}_{\text{tot}} = \vec{E}_{\text{inc}} + \vec{E}_{\text{rad}} + \vec{E}_{\text{ref}}$ . Here  $\vec{E}_{\text{inc}}$  represents the externally applied field in the presence of photonic structure;  $\vec{E}_{\text{rad}}$  represents the primary radiation field emitted by the TLS, before hitting any photonic structures;  $\vec{E}_{\text{ref}}$  represents the radiation field reflected after hitting photonic structure. In eq. (1), both  $\vec{E}_{\text{inc}}$  and  $\vec{E}_{\text{ref}}$  should be included in the driving term  $\vec{E}$  with no doubt. However, the  $\vec{E}_{\text{rad}}$  field produced by a dipole source is nonzero at its own position. Therefore, using the  $\vec{E}_{\text{tot}}$  field obtained from FDTD and substituting this value into eq. (1) results in the TLS being driven by the radiation field produced by itself. This leads to two effects: first, energy is carried away from TLS, causing it to decay at rate  $\Gamma_{\text{vac}}$ ; second, this self-interaction causes the TLS's resonance frequency to shift. This phenomenon, which can be understood as a numerical analogy of Lamb shift [53], has been observed in literatures [32, 33]. It is regarded as a numerical artifact that should be avoided.

To verify that  $\vec{E}_{\text{rad}}$  should not be included in the driving term, we now consider a simple example, where an incident pulse is scattered by a single TLS placed inside vacuum. It is well known that under weak-excitation limit, a TLS acts like an oscillating dipole [54]. Its scattering cross section  $\sigma(\omega)$  should follow a Lorentzian line shape, with maximum value  $\sigma_0 = \frac{3\lambda_0^2}{2\pi}$

and an FWHM of  $\Gamma_{\text{vac}}$  [55–59]. The simulation setup is shown schematically in Fig. 1(a). A Gaussian pulse with  $x$ -polarization serves as the incident wave, whose time-profile is plotted in the inset. The TLS, whose dipole moment  $|\langle g|\hat{d}|e\rangle| = 0.02$ , stays at its ground state  $|g\rangle$  at  $t = 0$ . The TLS is simulated using Bloch equation (see Appendix E for details), and four different scenarios are checked:

1. Decay rate  $\Gamma = 0$ ,  $\vec{E}_{\text{rad}}$  not excluded;
2. Decay rate  $\Gamma = 0$ ,  $\vec{E}_{\text{rad}}$  excluded;
3. Decay rate  $\Gamma = \Gamma_{\text{vac}}$ ,  $\vec{E}_{\text{rad}}$  not excluded (corresponds to most existing works);
4. Decay rate  $\Gamma = \Gamma_{\text{vac}}$ ,  $\vec{E}_{\text{rad}}$  excluded (corresponds to our proposed FDTD).

We surround the TLS with a power monitor to calculate the power of scattered electromagnetic field, then divide it by the incident light intensity to calculate the scattering cross section  $\sigma(\omega)$ . The results are summarized in the table shown in Fig. 1(a). Based on the first and the third rows, it can be concluded that if  $\vec{E}_{\text{rad}}$  is not excluded, the scattering cross section  $\sigma$  is much smaller than  $\sigma_0$  (noting that the  $\sigma(\omega)$  curves are exaggerated by  $400\times$ ). Also the resonance frequency shifts away from  $\omega_0$ . On the other hand, the second row shows that by setting  $\Gamma = 0$  and excluding  $\vec{E}_{\text{rad}}$ , the TLS's population  $P_e(t)$  does not decay, due to the lack of a decaying mechanism. As a comparison, our FDTD correctly recovers the position, linewidth, as well as the maximum value of the  $\sigma(\omega)$  peak. The exclusion of primary radiation  $\vec{E}_{\text{rad}}$  is essential for avoiding spurious self-interaction. Note that some researchers have tried to mimic TLS by modifying the dielectric constant  $\epsilon_r(\omega)$  of the grid point [33, 49]. Though the derivation of such dielectric function is well-known [60], it has been pointed out that this method does not exclude the self-interaction [31], making it incorrect when simulating isolated TLSs.

Based on the fact that a TLS should be driven by  $\vec{E}_{\text{inc}} + \vec{E}_{\text{ref}}$ , in the proposed FDTD we en-

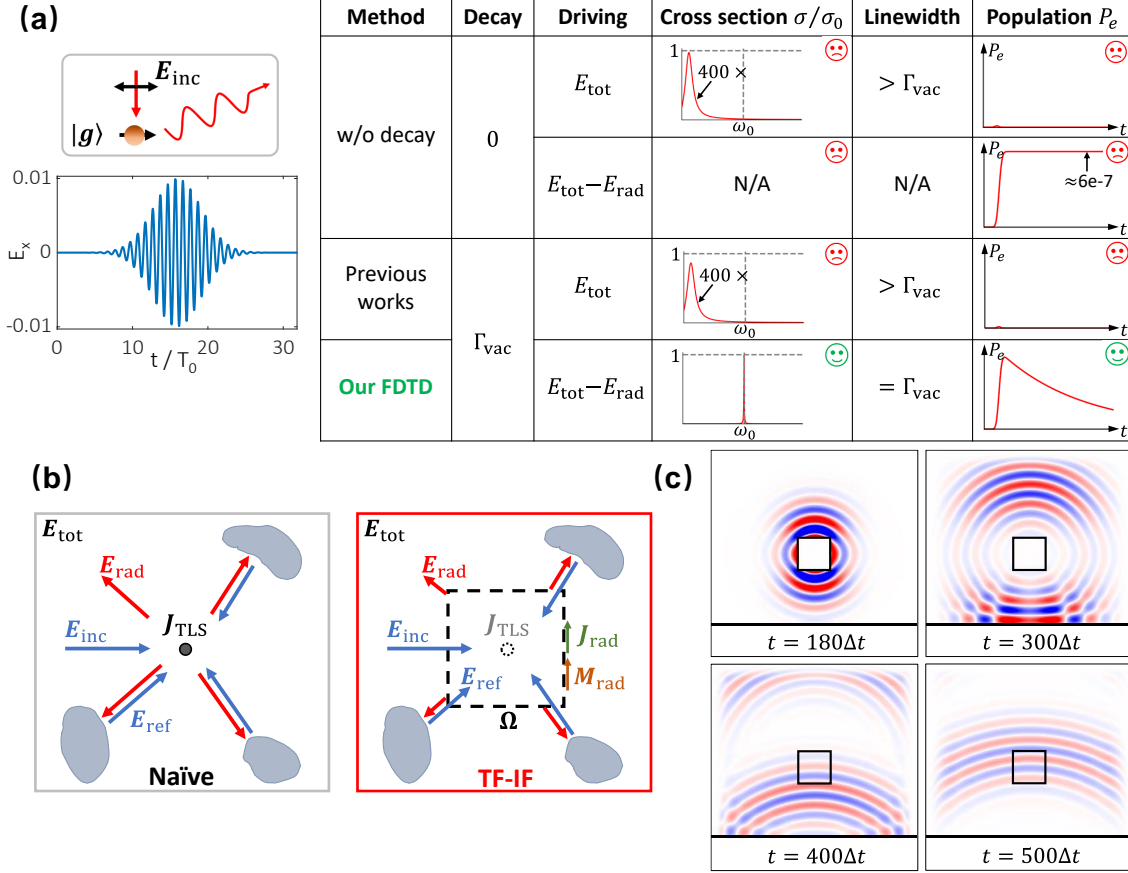


FIG. 1. The exclusion of primary radiation field produced by TLS. (a) Light scattering of one TLS inside vacuum. The inset shows the time profile of the incident Gaussian pulse. The table presents simulation results for 4 scenarios. Without excluding the radiation field  $\vec{E}_{\text{rad}}$ , the scattering cross section  $\sigma(\omega)$  cannot be predicted correctly. Our FDTD can get rid of the self-interaction caused by primary radiation, thus providing accurate results. (b) Comparison of the TF-IF technique with the naïve approach. When using TF-IF, the primary radiation  $\vec{E}_{\text{rad}}$  only exists outside region  $\Omega$ , making sure that unwanted self-interactions are eliminated. (c) The effect of TF-IF technique. An oscillating dipole in  $x$  direction is placed at the center of 3D domain. Nonzero  $E_x$  field is produced outside region  $\Omega$  (marked as a square box). After the radiation field has been reflected by a PEC mirror, it can enter  $\Omega$  and drive the oscillating dipole. Here  $\Delta t$  denotes the time step.

close the TLS with an imaginary square domain  $\Omega$ . We hope that the primary radiation field of this TLS only exists outside  $\Omega$ , thus the field  $\vec{E}$  sampled inside  $\Omega$  can be used to drive TLS. To achieve this, we utilize the surface equivalence principle [1, 61]: instead of directly using the TLS as a dipole source, ficti-

tious surface current densities are put on region boundary  $\partial\Omega$  (as shown in Fig. 1(b)), ensuring that the same radiation field is excited outside  $\Omega$ . We refer to this modification as total field-incident field (TF-IF) technique, which divides the simulation domain into different regions: within  $\Omega$  only the electromagnetic fields

incident from outside exist; outside  $\Omega$  the fields can be understood as “total field”  $\vec{E}_{\text{tot}}$ , including the primary radiation from the TLS. The modification and its name have been inspired by the total field-scattered field (TF-SF) technique, commonly used in FDTD simulations to generate incident wave [1]. The consequence of this TF-IF modification is depicted in Fig. 1(c). Here we consider a simple 3D FDTD simulation with a dipole source  $3\lambda_0$  above a PEC mirror. The dipole produces a pulse-like radiation field, and it is observed that the primary radiation field exists only outside region  $\Omega$  (marked by a square box). After the primary radiation field hits the mirror (marked by a black line) and gets reflected back, the reflected field  $\vec{E}_{\text{ref}}$  enters  $\Omega$  and re-excites the TLS. Therefore, the electric field sampled inside  $\Omega$  can be used directly as a driving term.

Our method is similar to the one proposed in [32]. Yet here our  $\Omega$  region can be much smaller (as small as  $3 \times 3 \times 3$  grid points) compared with the square region used in [32]. This flexibility is due to the radiation field being numerically calculated using an auxiliary FDTD (see Appendix D for details). This advantage enables us to model multiple TLSs that are placed very close (as close as the grid resolution  $\Delta x$ ) to each other, which will be demonstrated in the following sections. In contrast, simulations involving multiple TLSs are not presented in [32].

### B. Current source related to TLS radiation

In this section, we advance our discussion by considering a more general system containing  $N$  TLSs. The  $i$ -th TLS is located at position  $\vec{r}_i$  ( $i = 1, 2, \dots, N$ ). When utilizing FDTD, we focus on solving the following Maxwell’s equations:

$$\nabla \times \vec{E} = -\mu_0 \frac{\partial \vec{H}}{\partial t}, \quad (2)$$

$$\nabla \times \vec{H} = \epsilon_0 \frac{\partial \vec{E}}{\partial t} + \vec{J}_{\text{TLS}}. \quad (3)$$

While these equations describe electromagnetic fields in vacuum, it is straightforward to extend them to encompass complex photonic environments [1]. The conventional way to calculate the current source  $\vec{J}_{\text{TLS}}$  involves using the expectation value of dipole moment  $\langle \hat{d}_i \rangle$ :

$$\begin{aligned} \vec{J}_{\text{TLS}} &= \sum_i \frac{d}{dt} \langle \hat{d}_i \rangle \cdot \delta(\vec{r} - \vec{r}_i) \\ &= \sum_i \frac{d}{dt} \text{Tr}(\hat{d}_i \hat{\rho}_i) \cdot \delta(\vec{r} - \vec{r}_i), \end{aligned} \quad (4)$$

where  $\delta(\vec{r} - \vec{r}_i)$  denotes the Dirac  $\delta$ -function centered at  $\vec{r}_i$ , and  $\hat{\rho}_i$  stands for the density matrix of the  $i$ -th TLS. By using  $\langle \hat{d}_i \rangle$  as dipole source, all semi-classical methods attempt to simulate the expectation value of electric field  $\langle \hat{E} \rangle$ . Unfortunately, this procedure fails when considering spontaneous emission process, even for a single TLS. Starting from its excited state ( $\rho_{ee} = 1$ ) with zero coherence ( $\rho_{eg} = \rho_{ge} = 0$ ), the coherence  $\rho_{eg}(t)$  will remain zero during the decay process. Therefore, putting this dipole source  $\vec{J}_{\text{TLS}} \propto \frac{d}{dt} \langle \hat{d} \rangle \propto \frac{d}{dt} (\rho_{eg} + \rho_{ge}) = 0$  back into FDTD does not lead to any nonzero electromagnetic radiation [54]. This behavior is not surprising and has been highlighted by researchers [31, 62], noting that a single photon is radiated during the spontaneous emission process, and the expectation value of electric field  $\langle \hat{E} \rangle = 0$ . On the other hand the expectation value  $\langle \hat{E}^\dagger \hat{E} \rangle \neq 0$ , indicating that the probability of detecting a photon is nonzero. The quantum nature of a single photon leads to this paradox, making it impossible for existing semi-classical methods to model spontaneous emission.

To resolve the above issue, we adopt the theory developed in [63], focusing on the single-excitation state

$$|\Psi(t)\rangle = \sum_i b_i(t) |e_i, 0\rangle + \sum_{\vec{k}, \lambda} c_{\vec{k}\lambda}(t) |g, 1_{\vec{k}\lambda}\rangle, \quad (5)$$

where  $b_i(t)$  represents the  $i$ -th TLS’s excitation amplitude, and  $c_{\vec{k}\lambda}(t)$  corresponds to the

single-photon state with wave vector  $\vec{k}$  and polarization  $\lambda$ . Such single-excitation states, although simple, capture all phenomena in linear optics regime, and contain rich physics [9, 21, 24, 58, 64–68]. The ground state of this system is denoted as  $|\Psi_G\rangle = |g, 0\rangle$ . Instead of simulating  $\langle \vec{E} \rangle$ , we now use FDTD and simulate the time-evolution of the electric field  $\vec{E}(\vec{r}, t)$ , defined as [63]

$$\vec{E}(\vec{r}, t) = \langle \Psi(t) | \hat{\vec{E}}(\vec{r}) | \Psi_G \rangle + \langle \Psi_G | \hat{\vec{E}}(\vec{r}) | \Psi(t) \rangle, \quad (6)$$

which is nonzero for single-photon state, making it an ideal choice for simulating photon emission. The current source  $\vec{J}_{\text{TLS}}(\vec{r})$  that should be introduced in FDTD now becomes (see Appendix A)

$$\vec{J}_{\text{TLS}}(\vec{r}) = 2\omega_0 \sum_i \vec{d}_i \cdot \text{Im}(b_i) \cdot \delta(\vec{r} - \vec{r}_i), \quad (7)$$

where  $\text{Im}(b_i)$  stands for the imaginary part of  $b_i(t)$ .

To justify the above choices, we examine the spontaneous decay of an excited TLS inside vacuum. In Fig. 2(a) we compare our FDTD with two baseline semi-classical simulation techniques, namely, the Maxwell-Schrödinger equations and the Maxwell-Bloch equations (implementation details can be found in Appendix E). By plotting the time-evolution of the excited probability  $P_e$ , it is evident that the Schrödinger equation does not lead to spontaneous decay, and the TLS remains at the excited state, which is consistent with previous observations [28, 31, 69]. Both Bloch equation and our FDTD leads to an exponential decay as  $\exp(-\Gamma_{\text{vac}}t)$ . On the other hand, neither the Schrödinger equation nor the Bloch equation produces a nonzero  $\vec{E}$  field. This supports our assertion that the photon emission process cannot be simulated using semi-classical methods since  $\langle \vec{E} \rangle = 0$ . In contrast, by utilizing a different source as eq. (7), our proposed FDTD can accurately simulate the photon emission process.

### C. Process

Now we combine the two points mentioned previously, and briefly summarize the entire process of the proposed FDTD algorithm. We restrict our analysis to single-excitation quantum states defined in eq. (5). The  $\vec{E}(\vec{r}, t)$  field simulated in FDTD has been defined in eq. (6). By defining the  $\vec{H}(\vec{r}, t)$  field similarly, it can be proved that the time-evolution of these fields still follow classical Maxwell's equations (see Appendix A), and thus can be simulated using FDTD without any difficulty. On the other hand, the time-evolution of the  $i$ -th TLS's excitation amplitude  $b_i$  follows (see Appendix A)

$$\frac{db_i}{dt} = (-i\omega_0 - \frac{\Gamma_{\text{vac}}}{2})b_i + i \frac{\vec{d}_i \cdot \vec{E}(\vec{r}_i, t)}{\hbar}. \quad (8)$$

As previously stated,  $\vec{E}(\vec{r}_i)$  is sampled inside region  $\Omega_i$  and the primary radiation has been excluded. The above four equations, namely, eq. (2)(3)(7)(8), form the core of our proposed FDTD algorithm.

Before starting the FDTD simulation, we first initialize a 3D domain containing all photonic structures as well as all  $\Omega_i$  regions. The FDTD carried out in this domain is referred to as the “main FDTD”. Additionally, each TLS with index  $i$  requires an auxiliary FDTD to calculate the primary radiation fields ( $E_{i,\text{rad}}, H_{i,\text{rad}}$ ). These  $N$  FDTD simulations, filled with homogeneous media, are termed “auxiliary FDTD” and are kept small to minimize computational overhead (see Appendix D). At each time step, our proposed FDTD algorithm comprises 3 parts:

1. Update the main FDTD for one step, based on the current sources ( $\vec{J}_{i,\text{rad}}, \vec{M}_{i,\text{rad}}$ ) provided by auxiliary FDTDs.
2. Update all  $N$  TLSs for one step, using the  $\vec{E}(\vec{r}_i)$  field sampled from the main FDTD.
3. Update all  $N$  auxiliary FDTDs for one step, treating the TLSs as dipole sources.

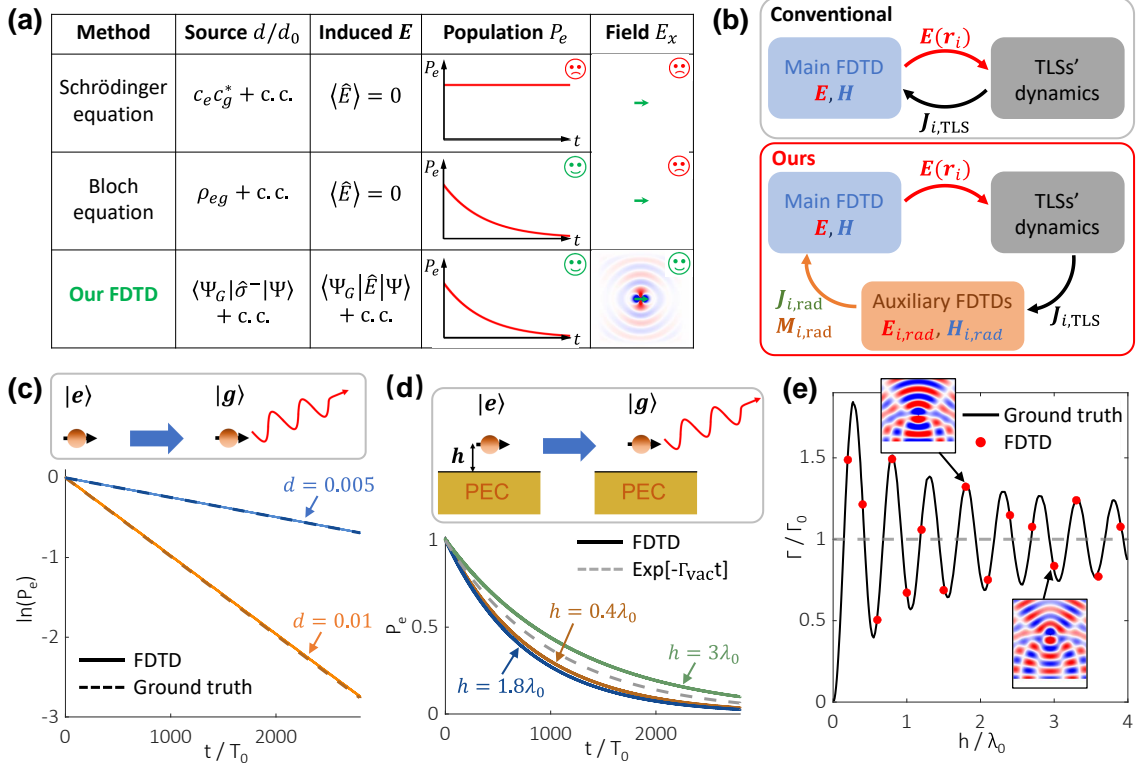


FIG. 2. Using a different current source to account for photon emission process. (a) Spontaneous emission of one TLS inside vacuum. Both Bloch equation and our FDTD recover an exponential decay in population. However the two semi-classical methods fail to produce nonzero fields since  $\langle \hat{E} \rangle = 0$ . (b) Flowchart of the proposed FDTD. The primary radiation of each TLS is calculated using an auxiliary FDTD. On the contrary, conventional methods do not exclude self-interaction. (c) Spontaneous emission of one TLS inside vacuum. (d) Spontaneous emission of one TLS placed above a PEC mirror. Time-evolution of  $P_e$  have been plotted for different distances  $h/\lambda_0 \in \{0.4, 1.8, 3\}$ . (e) The relationship between decay rate  $\Gamma$  and distance  $h$ . Results obtained by FDTD match perfectly with the ground truth. The insets show the corresponding  $H_z$  field distributions. Note that the simulations involved in (c)(d)(e) are carried out in 2D domain.

The above procedure has been illustrated in Fig. 2(b). Based on the surface equivalence principle [1, 61], the fictitious current sources ( $\vec{J}_{i,\text{rad}}, \vec{M}_{i,\text{rad}}$ ) used in the main FDTD are related to the primary radiation fields ( $\vec{E}_{i,\text{rad}}, \vec{H}_{i,\text{rad}}$ ) by:  $\vec{J}_{i,\text{rad}} = \hat{n} \times \vec{H}_{i,\text{rad}}$ ,  $\vec{M}_{i,\text{rad}} = -\hat{n} \times \vec{E}_{i,\text{rad}}$  (here  $\hat{n}$  denotes the normal vector of region surface  $\partial\Omega_i$ ). For more implementation details, please refer to Appendix D.

#### D. Spontaneous emission: $N = 1$ case

In this part, we provide several benchmark examples involving the spontaneous emission of  $N = 1$  TLS. The simplest case would be a TLS spontaneously decaying inside vacuum. Here we test two TLSs, with different dipole moments  $d \in \{0.005, 0.01\}$ . The time-evolution of excited probability  $P_e$  during the decay process is plotted in Fig. 2(c). It can be concluded that the proposed FDTD algorithm can reproduce

the exponential decay  $P_e(t) \sim \exp(-\Gamma_{\text{vac}}t)$ .

Next, to prove that our algorithm can capture the influence of photonic environment, we consider a TLS with dipole moment  $d_x = 0.01$ , located off a PEC mirror. The setup is shown in Fig. 2(d), with the distance between TLS and mirror denoted as  $h$ . In Fig. 2(d) we've plotted the time-evolution of  $P_e$  for three different cases,  $h = 0.4\lambda_0, 1.8\lambda_0, 3.0\lambda_0$ . Unlike Maxwell-Bloch equations, in which the spontaneous decay rate does not rely on environment, here the proposed FDTD give different curves for different  $h$  values. To verify that our FDTD can predict modified decay rates correctly, we further run multiple FDTD simulations for different heights  $h$ , ranging from  $0 \sim 4\lambda_0$ . The corresponding decay rates  $\Gamma$ , obtained through fitting  $P_e(t)$  with  $\exp(-\Gamma t)$ , are compared with analytical results in Fig. 2(e). As can be seen from the comparison, in all test cases our FDTD can predict the modified decay rate perfectly. By limiting ourselves to single-excitation states, the emission, reflection, as well as re-absorption of photon can be simulated correctly.

Note that it's not possible to arrive at the above results if semi-classical method is used to simulate a TLS starting from excited state, since a TLS with zero coherence cannot produce nonzero fields in FDTD. In that case, the spontaneous decay rate won't be affected by photonic structure, which is why many researchers tend to introduce a phenomenological parameter to compensate for the modified decay rate [10, 27, 30, 47, 49, 52]. In previous works, researchers often intentionally circumvent this issue, either by setting the initial state of the TLS as a superposition of the ground state and the excited state [49, 62, 70], or by using an incident pulse at the beginning to excite the TLS [26, 28–30, 52]. Our proposed FDTD can resolve this issue simply by restricting ourselves to single-excitation states. In this way we have successfully simulated the dynamics of the TLS when it gets re-excited by the reflected photon, leading to the correct modified decay rate.

### III. DIPOLE-DIPOLE INTERACTION: $N = 2$ CASE

Understanding photon exchange between TLSs (often referred to as resonant energy transfer) is fundamental to the development of modern quantum technologies [71–73]. This type of energy transfer also plays a crucial role in a variety of biological and chemical systems [74–77]. Given its importance, there have been substantial efforts to understand the underlying mechanisms of energy transport and to determine how these interactions can be controlled by engineering the photonic environment. In this section, we simulate the excitation transport process between two TLSs using our FDTD algorithm. At the beginning only the first TLS is at its excited state. After the first TLS emits a photon spontaneously, the second TLS can absorb this photon, leading to an increase of its excited probability. As discussed previously, a spontaneously decaying TLS with zero coherence cannot excite a nonzero classical electromagnetic field. Consequently, this process cannot be accurately modeled using semi-classical methods [62], such as the Maxwell-Bloch equations.

In our analysis, we compare the results of our FDTD simulations with those obtained from the master equation. This comparison has confirmed that our algorithm can simulate the excitation transport process with high accuracy. Furthermore, we have found that, since our FDTD does not rely on Markov approximation, it correctly captures the retardation effect caused by the finite traveling speed of photon. In contrast, the master equation approach under the Markov approximation fails to show this retardation effect, thereby violating causality.

#### A. Theory

In this section, we first review the theoretical framework governing the interaction between two TLSs within a photonic environment. Consider two such TLSs, where the  $i$ -th TLS ( $i = 1, 2$ ), characterized by a dipole moment  $\vec{d}_i$ ,



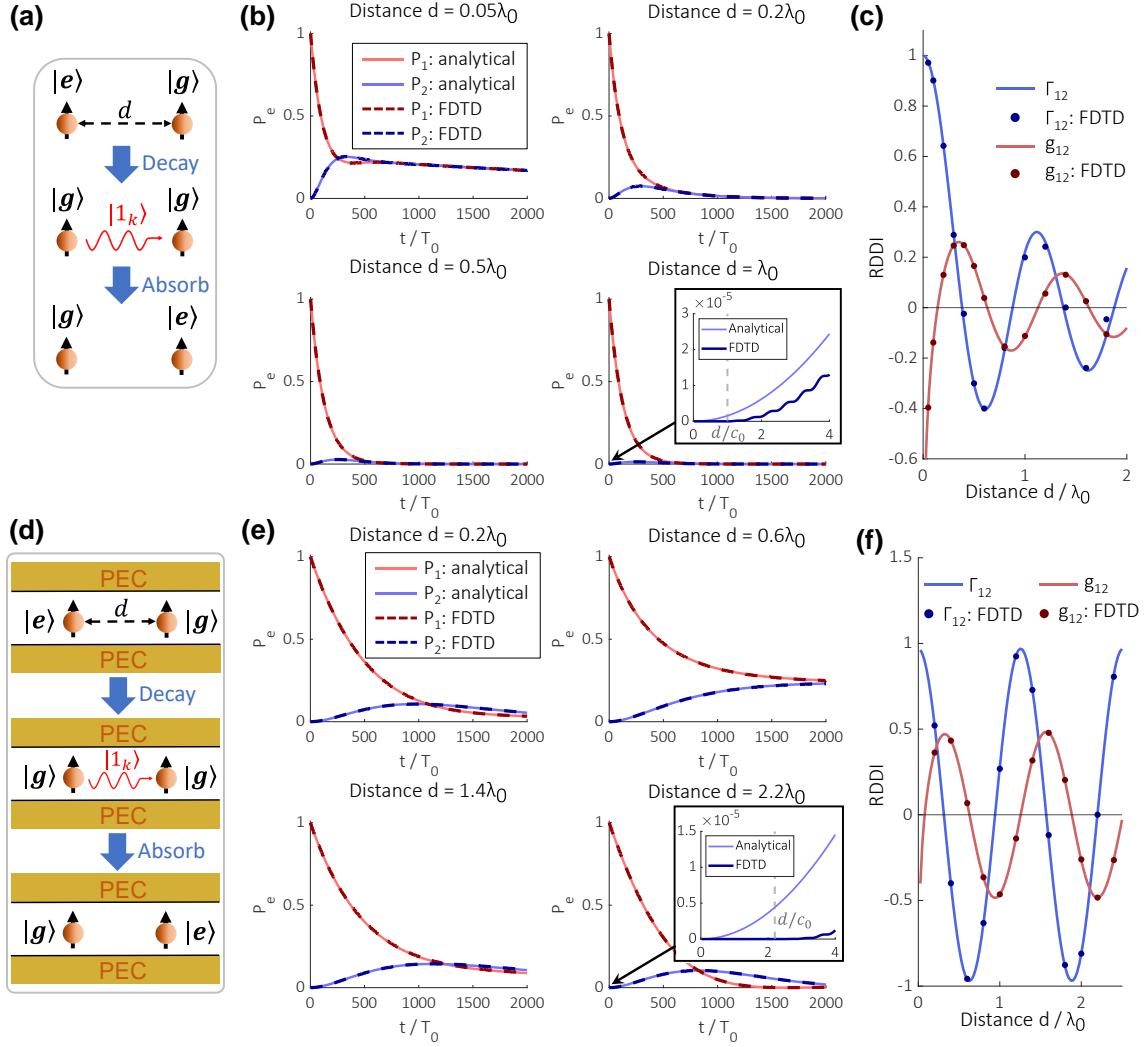


FIG. 3. 2D FDTD simulations involving  $N = 2$  TLSs, focusing on excitation transport between an excited TLS and an unexcited one. (a) Illustration of 2 TLSs placed inside vacuum. The excited TLS emits a photon, which can then be absorbed by the unexcited TLS. (b) The time-evolution of excited probabilities  $P_1(t)$  and  $P_2(t)$ . The inset shows that FDTD presents retardation effect and does not violate causality. (c) The dipole-dipole interaction strength (normalized by  $\Gamma_{\text{vac}}$ ) extracted from FDTD simulation. (d) Illustration of 2 TLSs placed at the middle of a waveguide, formed by 2 PEC mirrors. (e) The time-evolution of excited probabilities  $P_1(t)$  and  $P_2(t)$ . Similar to (b), the inset shows that FDTD presents retardation effect. (f) The dipole-dipole interaction strength (normalized by  $\Gamma_{\text{vac}}$ ) extracted from FDTD simulation. The interaction strength oscillates when increasing distance  $d$ , because emitted photon is confined by the waveguide.

is positioned at  $\vec{r}_i$ . The dipole-dipole interaction between these TLSs is evaluated based on the dyadic Green's function  $\vec{G}(\vec{r}_i, \vec{r}_j)$ :

$$\Gamma_{ij} = \frac{2\omega_0^2}{\hbar\epsilon_0 c_0^2} \vec{d}_i \cdot \text{Im} \vec{G}(\vec{r}_i, \vec{r}_j) \cdot \vec{d}_j, \quad (9)$$

$$g_{ij} = \frac{\omega_0^2}{\hbar\epsilon_0 c_0^2} \vec{d}_i \cdot \text{Re} \vec{G}(\vec{r}_i, \vec{r}_j) \cdot \vec{d}_j, \quad (10)$$

where  $\Gamma_{ij}$  represents the collective decay rate, and  $g_{ij}$  represents the coherent coupling.

We now focus on excitation transport and examine a more specific example: at  $t = 0$  only the first TLS is excited, while the second TLS is at its ground state, and there's no photon in the environment. The most commonly-used technique for solving this kind of system is the master equation. It has been demonstrated that [23, 65, 67, 78], after tracing out the photon degrees of freedom, the probabilities of finding these two TLSs in the excited state are

$$P_1(t) = \frac{1}{4} \left[ e^{-(\Gamma_{11} + \Gamma_{12})t} + e^{-(\Gamma_{11} - \Gamma_{12})t} \right] + \frac{e^{-\Gamma_{11}t}}{2} \cos(2g_{12}t), \quad (11)$$

$$P_2(t) = \frac{1}{4} \left[ e^{-(\Gamma_{11} + \Gamma_{12})t} + e^{-(\Gamma_{11} - \Gamma_{12})t} \right] - \frac{e^{-\Gamma_{11}t}}{2} \cos(2g_{12}t). \quad (12)$$

From the above equations, it is evident that the analytical solution overlooks the retardation effect [34, 36]. In the subsequent section, we will compare our FDTD simulation results with the above analytical solutions eq. (11)(12), and show that FDTD successfully accounts for the finite traveling speed of light.

## B. Simulation results and comparison

In this section we present the FDTD simulation results for two different 2D test cases. In

the first scenario, two identical TLSs with resonance wavelength  $\lambda_0 = 1 \mu\text{m}$  are positioned within a vacuum environment, as depicted in Figure 3(a). In the second scenario, the same TLSs are placed inside a waveguide formed by two parallel PEC boards, as illustrated in Fig. 3(d). The separation distance between TLS 1 and TLS 2 is denoted as  $d$ . By setting the initial condition as  $b_1(t = 0) = 1$ ,  $b_2(t = 0) = 0$ , our modified FDTD approach can accurately simulate the photon emission from the first TLS as well as the photon absorption by the second TLS.

For the vacuum case, the time-evolution of excited probabilities  $P_1(t)$  and  $P_2(t)$  are depicted using dashed lines (see Fig. 3(b)). The corresponding analytical solutions derived from the master equation are also plotted for comparison. We have explored four different inter-TLS distances,  $d/\lambda_0 \in \{0.05, 0.2, 0.5, 1\}$ , and our FDTD results agree pretty well with analytical results eq. (11)(12) for all different distances. For the case where  $d = \lambda_0$ , an inset has been added to show a detailed view of  $P_2(t)$  over the time interval  $t \in [0, 4T_0]$ . While the solution from the master equation becomes nonzero immediately after  $t = 0$ , the  $P_2(t)$  obtained from FDTD remains zero until  $t_r = d/c_0$  (highlighted by a dashed gray line). It is not surprising that FDTD simulation can model retardation effect correctly, since wave travels with finite speed  $c_0$  in FDTD. To verify the accuracy of our FDTD algorithm, we estimate the corresponding collective decay rate  $\Gamma_{12}$  and the coherent coupling  $g_{12}$ , based on the  $P_1(t)$ ,  $P_2(t)$  curves obtained from FDTD simulations. The estimation is carried out through a curve fitting process based on the form of analytical solution eq. (11)(12). The comparison between the estimated values and ground truth is shown in Fig. 3(c). It can be concluded that FDTD maintains high accuracy across most test scenarios. In contrast, although the semi-classical method introduced in [62] can capture the retardation effect, it does not accurately determine the dipole-dipole interaction strength.

The above examples do not involve non-trivial photonic environment beyond vacuum.

To prove that our FDTD handles the dipole-dipole interaction correctly with the presence of photonic structures, we introduce a second test case featuring a waveguide formed by two parallel PEC mirrors. The width of this waveguide is  $w = 0.8\lambda_0$ , and the two TLSs are placed at the center of the PEC waveguide, as depicted in Fig. 3(d). Similar to the previous test case, we obtain the time-evolution of excited probabilities  $P_1(t)$  and  $P_2(t)$  from FDTD simulation across four different distances  $d/\lambda_0 \in \{0.2, 0.6, 1.4, 2.2\}$ . In Fig. 3(e), the FDTD results are plotted using dashed lines, while the corresponding solutions obtained from master equation are also plotted for comparison. Once again, our FDTD agrees well with the analytical solutions under all tested conditions. Notably, for the  $d = 2.2\lambda_0$  case, an inset has been included, showing  $P_2(t)$  for time  $t \in [0, 4T_0]$ . A gray dashed line marks  $t_r = d/c_0$ , and serves as reference for the earliest time before photon can reach the second TLS. While FDTD shows the retardation effect, the master equation gives nonzero  $P_2$  for all  $t > 0$ , which violates causality. Similar to the vacuum test case, the  $\Gamma_{12}$  and  $g_{12}$  coefficients are extracted from  $P_1(t)$ ,  $P_2(t)$  with the help of curve fitting process. We compare the estimated values with ground truth obtained from dyadic Green's function, and the results are presented in Fig. 3(f). Notice that due to the waveguide's confinement effect, the dipole-dipole interaction does not decay quickly with increased distance  $d$  but instead oscillates in a sinusoidal manner.

In conclusion, the proposed FDTD algorithm effectively simulates the excitation transport between two TLSs, which is difficult to achieve using semi-classical methods [62]. Our FDTD method not only captures the complex dipole-dipole interactions across varying distances and environments, but also demonstrates significant computational efficiency, especially as the number of TLSs,  $N$ , increases. Unlike the master equation approach, which requires computing all  $\Gamma_{ij}$  and  $g_{ij}$  coefficients before starting simulation, for FDTD the explicit calculation of  $\Gamma_{ij}$  and  $g_{ij}$  coefficients is easily avoided. Instead, the dynamics of the entire system can be re-

trieved from a single FDTD run, offering a more scalable technique.

#### IV. COLLECTIVE BEHAVIOR OF TLS CLUSTER

In the previous sections, we have provided several benchmark examples involving  $N = 1$  and  $N = 2$  TLSs, which substantiate the accuracy of our algorithm and highlight its advantage over existing algorithms. In this section, we demonstrate the scalability of our proposed algorithm by simulating the collective behavior of  $N > 2$  TLSs within a 3D domain. We select two representative scenarios: the Dicke superradiance in an ordered TLS array within vacuum, and Rabi splitting induced by coupling multiple TLSs with a ring resonator. To the best of our knowledge, this study is the first to correctly incorporate multiple isolated TLSs into a 3D FDTD simulation. Many previous studies have focused on ensembles of TLSs, allowing them to safely ignore self-interaction [26, 27, 46, 47, 51, 79]; however, some papers that claim to simulate isolated TLS have overlooked self-interaction, leading to results that are qualitatively incorrect [28, 29, 49, 50, 52]. While only a few studies have successfully integrated isolated TLS into FDTD with self-interactions correctly excluded, simulations involving multiple TLSs are still missing [30, 32, 33, 48]. In the subsequent sections, we demonstrate that with TLSs incorporated, FDTD not only validates known phenomena, but also reveals phenomena that may have been overlooked in prior research. This is because the proposed FDTD method minimizes reliance on commonly used approximations, including the single-mode approximation, rotating-wave approximation (RWA), and Markov approximation.

##### A. Superradiance of ordered TLS array

In this part we consider the superradiance phenomenon of an ordered TLS array in vacuum [80, 81]. As is well known, TLSs in close

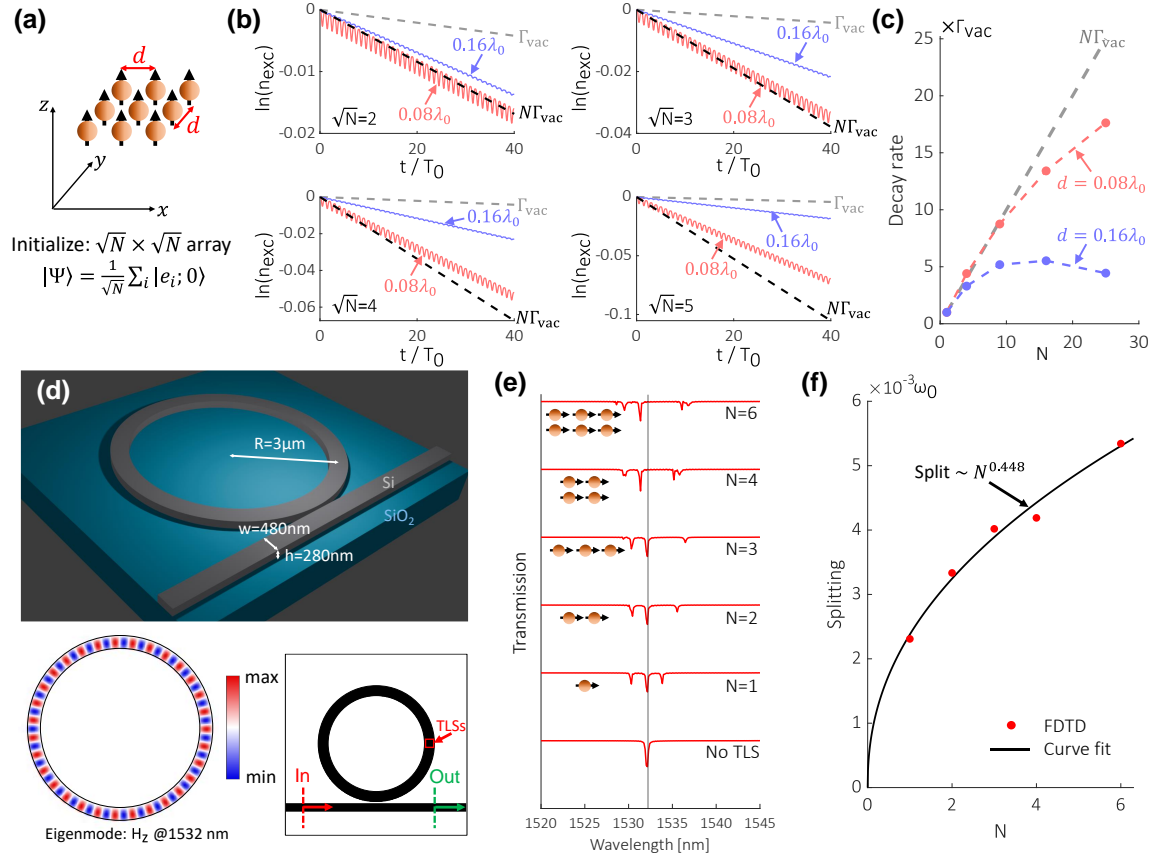


FIG. 4. 3D FDTD simulations involving  $N > 2$  TLSs. Two examples, namely superradiance and strong-coupling cavity QED, are included. (a) Illustration of the simulated square TLS array. The distance between neighboring TLSs is denoted as  $d$ . All dipole moments are aligned at  $z$  direction. (b) Time-evolution of the total excitation number  $n_{exc}$ , under different array sizes and TLS spacings.  $\exp(-\Gamma_{vac}t)$  and  $\exp(-N\Gamma_{vac}t)$  are shown in dashed lines for comparison. Compact arrays show decay rates that are very close too  $N\Gamma_{vac}$ , while more extended arrays decay slower. (c) The corresponding decay rates extracted through curve fitting. (d) Illustration of the 3D ring resonator used in cavity QED simulation. The first inset plots the  $H_z$  distribution of one eigenmode. The second inset shows the input port, output port, as well as the position of TLSs. (e) The transmission spectra when  $N$  TLSs are strongly coupled to the ring resonator. Here  $N \in \{0, 1, 2, 3, 4, 6\}$ . Mode splitting becomes larger when more TLSs are coupled to the resonator. Notice that when  $N \geq 3$  more than 3 dips exist in the transmission curve. (f) The relationship between measured Rabi splitting and number  $N$ . Curve fitting shows that the splitting is proportional to  $N^{0.448}$ , which increases slightly slower compared to the ideal  $\sqrt{N}$  scaling predicted by single-mode cavity QED.

proximity to each other interact with light collectively. These TLSs tend to synchronize as they decay, resulting in a fast decay rate that is  $N$  times larger than that of a single TLS

[68, 82, 83]. Such superradiance phenomenon was first predicted by R. Dicke in 1954 [84], and has already been observed in a wide range of experimental systems [85–87]. However, nu-

merical simulation of such phenomenon based on FDTD are rarely reported [88]. The simulation setup is shown schematically in Fig. 4(a). A square array consisting of  $N$  TLSs is positioned at the  $z = 0$  plane. All TLSs feature a dipole moment oriented in the  $z$  direction, each with a magnitude of 0.002. The distance between neighboring TLSs is denoted as  $d$ , and in our simulations two different distances  $d/\lambda_0 \in \{0.08, 0.16\}$  have been tested. Given that our method focuses on single-excitation states, the initial quantum state of the system is set as  $|\Psi(t=0)\rangle = \frac{1}{\sqrt{N}} \sum_i |e_i, 0\rangle$ . We record the total number of excitations  $n_{\text{exc}}$ , defined as the sum of the excited probabilities  $|b_i|^2$ . The time-evolution of logarithm  $\ln(n_{\text{exc}})$  is plotted in Fig. 4(b). For comparison, the exponential decay curve of an isolated TLS,  $\exp(-\Gamma_{\text{vac}}t)$ , is shown in gray dashed lines. Additionally, the black dashed line showing  $\exp(-N\Gamma_{\text{vac}}t)$  represents the ideal case of superradiance, where all TLSs are in close proximity and oscillate in-phase.

Four different array sizes ( $N = 2 \times 2, 3 \times 3, 4 \times 4$  and  $5 \times 5$ ) have been examined. As previously mentioned, our FDTD does not rely on RWA, leading to fast oscillations in the  $n_{\text{exc}}$  curve. It can be concluded that when the array is confined within a region much smaller than the wavelength  $\lambda_0$ ,  $n_{\text{exc}}$  decays with a rate very close to  $N\Gamma_0$ . Conversely, when the array size is comparable to  $\lambda_0/2$ , TLSs at different locations cannot oscillate perfectly in-phase, resulting in a decay rate smaller than  $N\Gamma_{\text{vac}}$ . Through curve fitting, we have extracted the decay rates from all  $n_{\text{exc}}(t)$  curves, and these results are displayed in Fig. 4(c). It's evident that when neighboring TLSs are close to each other ( $d = 0.08\lambda_0$  case), the decay rate only deviates from  $N\Gamma_0$  significantly when  $N$  becomes larger than 16. However, for larger spacing  $d = 0.16\lambda_0$ , the decay rate ceases to increase once  $N > 9$ . Our simulation results align with recent studies [80, 81], suggesting that superradiance in an ordered TLS array only occurs when the inter-TLS distance is below a critical value.

## B. Rabi splitting in cavity

A cavity quantum electrodynamics (cavity QED) system is crucial, as it not only facilitates the study of fundamental physics, but also provides a platform for quantum information processing [17, 89–91]. To date, numerical simulations relevant to this topic are mostly based on cavity QED theory, typically considering only a few cavity modes (often just a single mode) [18, 20]. Although these simulation techniques are straightforward to implement, they become inadequate when the photonic environment or the placement of TLSs becomes increasingly complex. In this section, we demonstrate the versatility of our algorithm by simulating multiple TLSs strongly coupled to a ring resonator. We consider a silicon ring resonator placed on top of a silica substrate, as depicted in Fig. 4(d). The ring resonator is coupled to an adjacent silicon waveguide, positioned 80 nm from the ring. Additional size parameters are provided in Fig. 4(d). The ring resonator features a free spectral range (FSR) of approximately 369 THz. The magnetic field distribution  $H_z$  for one eigenmode at 1532 nm is illustrated in Fig. 4. Multiple TLSs, with dipole moments oriented in  $x$  direction, are embedded within the ring resonator. As shown by the insets of Fig. 4(e), these TLSs form an array, which is centered at position  $(R, 0, 0)$ . The distance between neighboring TLSs remain fixed as  $d = 0.08\lambda_0$ .

The TE<sub>0</sub> waveguide mode is injected from the input port (indicated in red) on the left side, and the transmission through the system is measured at the output port (indicated in green) on the right side. The corresponding transmission spectra for different number of TLSs  $N \in \{0, 1, 2, 3, 4, 6\}$  are depicted in Fig. 4(e). The resonance wavelength  $\lambda_0$  is highlighted with a vertical line. In the absence of TLSs, the transmission spectrum features a single dip. Coupling a single TLS ( $N = 1$ ) with the ring resonator results in three dips. This effect arises because the ring resonator supports two degenerate cavity modes: one traveling clockwise (CW) and the other counter-clockwise

(CCW). With a dipole moment of 0.01 oriented in the  $x$  direction, the TLS interacts with both CW and CCW modes, leading to the splitting of three distinct modes. This phenomenon, known as vacuum Rabi splitting [92], indicates that the dipole moment is sufficiently large to achieve the strong-coupling regime. As the number of TLSs coupled with the ring resonator increases, the mode splitting becomes larger. The relationship between splitting (measured by subtracting the frequencies of two most distant dips) and the number of TLSs  $N$  is plotted in Fig. 4(f). According to cavity QED theory, when  $N$  TLSs are coupled to a single cavity mode, the Rabi splitting should scale as  $\sqrt{N}$  [87, 93, 94]. In our simulations, the relationship between splitting and  $N$  has been determined through curve fitting. Our FDTD simulations reveal that the splitting is proportional to  $N^{0.448}$ , which is slightly lower compared to the theoretical  $N^{0.5}$  scaling. This deviation can be attributed to the inter-TLS distance  $d = 0.08\lambda_0$ , which results in variations in the coupling constants among different TLSs.

One thing worth paying attention to is that, for all cases with  $N \geq 3$ , more than 3 dips appear in the transmission spectra. This observation might seem counter-intuitive, as single-mode cavity QED theory predicts that the number of transmission dips (or peaks) should not increase with  $N$ . We speculate that these additional dips correspond to eigenmodes typically referred to as “dark states” [7]. These dark states are not entirely “dark” when considering the near-field coupling between TLSs [56, 58, 95, 96], an interaction that is overlooked in conventional single-mode cavity QED treatments [97]. We are currently trying to gain a deeper understanding of these unexpected quantum states. Exploring the potential applications of these dark states would be an intriguing direction for future research.

## V. CONCLUSION

In this work, we aim to incorporate quantum TLSs into well-developed FDTD simula-

tion framework. This integration provides a methodology to analyze the behavior of multiple TLSs within various photonic environments. We realized that many existing simulation techniques employ semi-classical approaches, and cannot even simulate the emission of photon from an excited TLS. Additionally, these techniques often fail to correctly exclude primary radiation fields, resulting in spurious frequency shifts. Our efforts to address the above issues are two-fold: theoretically, we restrict our analysis to single-excitation quantum states, which has allowed us to precisely define the current sources for modeling photon emission; numerically, we introduce the TF-IF technique, utilizing auxiliary FDTDs to exclude primary radiation fields. By making the above modifications, we have enabled the simulation of TLS dynamics within complex photonic environments, with spurious self-interactions eliminated. This paper presents several test cases to validate the accuracy of our FDTD algorithm. For a single TLS ( $N = 1$ ) we have confirmed that our FDTD accurately simulates both photon scattering and spontaneous emission. For two TLSs we focus on the excitation transport between two distant TLSs. Notably, our FDTD simulations reproduce the retardation effects due to the finite speed of light, thereby maintaining causality, a feature often neglected in simulations based on Markov approximation. To further demonstrate the scalability of our algorithm, we have included two more examples involving  $N > 2$  TLSs. Based on the results, our FDTD can correctly simulate superradiance effect of TLS array, as well as vacuum Rabi splitting when multiple TLSs couple strongly with a ring resonator.

In summary, the proposed FDTD algorithm accurately captures a variety of phenomena that are of great interest to researchers. Additionally, FDTD can predict novel behaviors that have been overlooked in past research works, due to the use of various simplifications. Our FDTD is scalable when the number of TLSs increases, because the overhead is caused by introducing auxiliary FDTDs, which are much smaller in size compared with the main FDTD.

The algorithm has been implemented using CUDA C++, with the code made publicly available on [GitHub](#). We are confident that our modified FDTD will serve as a powerful tool, bridging the gap between theoretical predictions and experimental verifications: theorists can test their hypotheses without physical experiments, while experimentalists gain a more realistic simulation platform that can predict outcomes prior to laboratory experiments. Despite these advantages, our FDTD still relies on the assumption of single-excitation states, which limits its application to quantum systems with multiple excitations. Investigating whether similar numerical techniques could be adapted to systems containing multiple entangled TLSs and photons would be a promising direction for future research.

Currently, we are in the process of integrating this algorithm into Tidy3d [2], a well-regarded FDTD simulation platform, with the aim of making it accessible to the research community shortly. As part of our long-term objectives,

we plan to enhance the proposed technique to encompass more complex quantum emitters, including atoms and molecules with multiple energy levels. A simulation technique that can accurately simulate the dynamics of molecular interactions inside complex environments is highly desired. We anticipate that the development of such tool will significantly advance research and enhance our understanding across a wide range of fields, including quantum physics, chemistry, as well as biology.

## ACKNOWLEDGMENTS

The authors would like to acknowledge Prof. Jennifer T. Choy, Prof. Shimon Kolkowitz, Momchil Minkov, as well as Boyuan Liu for many helpful discussions. This work was supported by National Science Foundation’s QLCI-CI: Hybrid Quantum Architectures and Networks.

## Appendix A: Derivation of equations of motion

In this part, we derive the equations of motion presented in “theoretical foundation” part of the main text. For the sake of clarity, we start by defining the system Hamiltonian. Consider a system containing  $N$  TLSs. Suppose the  $i$ -th TLS is placed at position  $\vec{r}_i$ , and its dipole moment is  $\vec{d}_i$ . The Hamiltonian of this quantum system consists of three parts:  $\hat{H} = \hat{H}_{\text{TLS}} + \hat{H}_{ph} + \hat{H}_{\text{int}}$ , where  $\hat{H}_{\text{TLS}}$  stands for the TLS part,  $\hat{H}_{ph}$  stands for the photon part, and  $\hat{H}_{\text{int}}$  stands for the interaction. These three parts can be explicitly written as follows:

$$\hat{H}_{\text{TLS}} = \sum_i \hbar\omega_0 \hat{\sigma}_i^+ \hat{\sigma}_i^-, \quad (\text{A1})$$

$$\hat{H}_{ph} = \sum_{\vec{k}} \hbar\omega_{\vec{k}} \hat{a}_{\vec{k}}^\dagger \hat{a}_{\vec{k}}, \quad (\text{A2})$$

$$\hat{H}_{\text{int}} = - \sum_i (\hat{\sigma}_i^+ + \hat{\sigma}_i^-) \vec{d}_i \cdot \vec{E}(\vec{r}_i), \quad (\text{A3})$$

where  $\omega_0$  stands for the resonance frequency of TLS,  $\hat{\sigma}_i^+$  ( $\hat{\sigma}_i^-$ ) stands for the raising (lowering) operator of the  $i$ -th TLS;  $\omega_{\vec{k}}$  and  $\hat{a}_{\vec{k}}^\dagger$  ( $\hat{a}_{\vec{k}}$ ) are the frequency and raising (lowering) operator of the corresponding plane-wave mode.

As stated in the main text, we consider the time-evolution of single-excitation state

$$|\Psi(t)\rangle = \sum_i b_i(t)|e_i, 0\rangle + \sum_{\vec{k}, \lambda} c_{\vec{k}\lambda}(t)|g, 1_{\vec{k}\lambda}\rangle. \quad (\text{A4})$$

### 1. Definition of $\vec{E}$ and $\vec{B}$ fields

When quantizing the electromagnetic wave, the definition of operator  $\hat{\vec{E}}$  and  $\hat{\vec{B}}$  can be written as [54]:

$$\begin{aligned} \hat{\vec{E}}(\vec{r}) &= i \sum_{\vec{k}, \lambda} \sqrt{\frac{\hbar\omega_k}{2V\epsilon_0}} \cdot \left( \vec{\epsilon}_{\vec{k}\lambda} \hat{a}_{\vec{k}\lambda} e^{i\vec{k}\cdot\vec{r}} - \vec{\epsilon}_{\vec{k}\lambda}^\dagger \hat{a}_{\vec{k}\lambda}^\dagger e^{-i\vec{k}\cdot\vec{r}} \right), \\ \hat{\vec{B}}(\vec{r}) &= i \sum_{\vec{k}, \lambda} \sqrt{\frac{\hbar}{2V\epsilon_0\omega_k}} \cdot (\vec{k} \times \vec{\epsilon}_{\vec{k}\lambda}) \cdot \left( \hat{a}_{\vec{k}\lambda} e^{i\vec{k}\cdot\vec{r}} - \hat{a}_{\vec{k}\lambda}^\dagger e^{-i\vec{k}\cdot\vec{r}} \right). \end{aligned} \quad (\text{A5})$$

Since we focus on single-excitation state, we follow [63] and define  $\vec{E}(\vec{r}, t)$ ,  $\vec{B}(\vec{r}, t)$  fields in the following way:

$$\begin{aligned} \vec{E}(\vec{r}, t) &= \langle \Psi(t) | \hat{\vec{E}}(\vec{r}) | \Psi_G \rangle + \langle \Psi_G | \hat{\vec{E}}(\vec{r}) | \Psi(t) \rangle, \\ \vec{B}(\vec{r}, t) &= \langle \Psi(t) | \hat{\vec{B}}(\vec{r}) | \Psi_G \rangle + \langle \Psi_G | \hat{\vec{B}}(\vec{r}) | \Psi(t) \rangle. \end{aligned} \quad (\text{A6})$$

Now we first need to relate the above field quantities to  $c_{\vec{k}\lambda}(t)$  coefficients. For  $\vec{E}(\vec{r}, t)$  this can be derived as

$$\begin{aligned} \vec{E}(\vec{r}, t) &= \langle \Psi_G | \hat{\vec{E}}(\vec{r}) | \Psi(t) \rangle + c.c. \\ &= \langle g, 0 | i \sum_{\vec{k}, \lambda} \sqrt{\frac{\hbar\omega_k}{2V\epsilon_0}} \cdot \vec{\epsilon}_{\vec{k}\lambda} \left( \hat{a}_{\vec{k}\lambda} e^{i\vec{k}\cdot\vec{r}} - \hat{a}_{\vec{k}\lambda}^\dagger e^{-i\vec{k}\cdot\vec{r}} \right) | \Psi(t) \rangle + c.c. \\ &= \langle g, 0 | i \sum_{\vec{k}, \lambda} \sqrt{\frac{\hbar\omega_k}{2V\epsilon_0}} \cdot \vec{\epsilon}_{\vec{k}\lambda} c_{\vec{k}\lambda}(t) e^{i\vec{k}\cdot\vec{r}} | g, 0 \rangle + c.c. \\ &= i \sum_{\vec{k}, \lambda} \sqrt{\frac{\hbar\omega_k}{2V\epsilon_0}} \cdot \vec{\epsilon}_{\vec{k}\lambda} \left[ c_{\vec{k}\lambda}(t) e^{i\vec{k}\cdot\vec{r}} - c_{\vec{k}\lambda}^*(t) e^{-i\vec{k}\cdot\vec{r}} \right]. \end{aligned} \quad (\text{A7})$$

Similar results can be derived for  $\vec{B}(\vec{r}, t)$ :

$$\vec{B}(\vec{r}, t) = i \sum_{\vec{k}, \lambda} \sqrt{\frac{\hbar}{2V\epsilon_0\omega_k}} (\vec{k} \times \vec{\epsilon}_{\vec{k}\lambda}) \cdot \left[ c_{\vec{k}\lambda}(t) e^{i\vec{k}\cdot\vec{r}} - c_{\vec{k}\lambda}^*(t) e^{-i\vec{k}\cdot\vec{r}} \right]. \quad (\text{A8})$$

We will now prove that the time-evolution of  $\vec{E}$  and  $\vec{B}$  fields defined above follow Maxwell's equations:

$$\frac{1}{c_0^2} \frac{\partial \vec{E}}{\partial t} = \nabla \times \vec{B}, \quad (\text{A9})$$



$$\frac{\partial \vec{B}}{\partial t} = -\nabla \times \vec{E}. \quad (\text{A10})$$

Note that the above equations are source-free, and the current sources provided by TLS will be added later.

For eq. (A9), the left hand side can be derived as

$$\begin{aligned} \frac{1}{c_0^2} \frac{\partial \vec{E}}{\partial t} &= \frac{i}{c_0^2} \sum_{\vec{k}, \lambda} \sqrt{\frac{\hbar \omega_k}{2V \epsilon_0}} \vec{\epsilon}_{\vec{k}\lambda} \left[ \frac{dc_{\vec{k}\lambda}}{dt} e^{i\vec{k}\cdot\vec{r}} - \frac{dc_{\vec{k}\lambda}^*}{dt} e^{-i\vec{k}\cdot\vec{r}} \right] \\ &= \frac{i}{c_0^2} \sum_{\vec{k}, \lambda} \sqrt{\frac{\hbar \omega_k}{2V \epsilon_0}} \vec{\epsilon}_{\vec{k}\lambda} \left[ -i\omega_k c_{\vec{k}\lambda} e^{i\vec{k}\cdot\vec{r}} - c.c. \right] \\ &= \sum_{\vec{k}, \lambda} \frac{1}{c_0^2} \sqrt{\frac{\hbar}{2V \epsilon_0}} \cdot \omega_k^{3/2} \vec{\epsilon}_{\vec{k}\lambda} (c_{\vec{k}\lambda} e^{i\vec{k}\cdot\vec{r}} + c.c.), \end{aligned} \quad (\text{A11})$$

while the right hand side is

$$\begin{aligned} \nabla \times \vec{B} &= - \sum_{\vec{k}, \lambda} \sqrt{\frac{\hbar}{2V \epsilon_0 \omega_k}} \cdot \left[ (\vec{k} \times \vec{k} \times \vec{\epsilon}_{\vec{k}\lambda}) c_{\vec{k}\lambda} e^{i\vec{k}\cdot\vec{r}} + c.c. \right] \\ &= \sum_{\vec{k}, \lambda} \sqrt{\frac{\hbar}{2V \epsilon_0 \omega_k}} \cdot k^2 \vec{\epsilon}_{\vec{k}\lambda} \cdot (c_{\vec{k}\lambda} e^{i\vec{k}\cdot\vec{r}} + c.c.) \\ &= \sum_{\vec{k}, \lambda} \frac{1}{c_0^2} \sqrt{\frac{\hbar}{2V \epsilon_0}} \cdot \omega_k^{3/2} \vec{\epsilon}_{\vec{k}\lambda} (c_{\vec{k}\lambda} e^{i\vec{k}\cdot\vec{r}} + c.c.). \end{aligned} \quad (\text{A12})$$

Thus eq. (A9) has been proved.

Eq. (A10) is treated in a similar manner. The left hand side can be expressed as

$$\begin{aligned} \frac{\partial \vec{B}}{\partial t} &= i \sum_{\vec{k}, \lambda} \sqrt{\frac{\hbar}{2V \epsilon_0 \omega_k}} (\vec{k} \times \vec{\epsilon}_{\vec{k}\lambda}) \cdot \left[ \frac{dc_{\vec{k}\lambda}}{dt} e^{i\vec{k}\cdot\vec{r}} - \frac{dc_{\vec{k}\lambda}^*}{dt} e^{-i\vec{k}\cdot\vec{r}} \right] \\ &= \sum_{\vec{k}, \lambda} \sqrt{\frac{\hbar}{2V \epsilon_0}} \omega_k^{1/2} \cdot (\vec{k} \times \vec{\epsilon}_{\vec{k}\lambda}) \cdot (c_{\vec{k}\lambda} e^{i\vec{k}\cdot\vec{r}} + c.c.). \end{aligned} \quad (\text{A13})$$

The right hand side is

$$\begin{aligned} -\nabla \times \vec{E} &= -i \sum_{\vec{k}, \lambda} \sqrt{\frac{\hbar \omega_k}{2V \epsilon_0}} \cdot (i\vec{k} \times \vec{\epsilon}_{\vec{k}\lambda}) \cdot (c_{\vec{k}\lambda} e^{i\vec{k}\cdot\vec{r}} + c.c.) \\ &= \sum_{\vec{k}, \lambda} \sqrt{\frac{\hbar}{2V \epsilon_0}} \omega_k^{1/2} \cdot (\vec{k} \times \vec{\epsilon}_{\vec{k}\lambda}) \cdot (c_{\vec{k}\lambda} e^{i\vec{k}\cdot\vec{r}} + c.c.), \end{aligned} \quad (\text{A14})$$

which is equivalent to the left hand side, proving the validity of eq. (A10).

The above proof verifies that the time-evolution of real fields  $\vec{E}(\vec{r}, t)$ ,  $\vec{H}(\vec{r}, t)$  defined in the main text follow Maxwell's equations. The result is consistent with the derivation presented in [63], indicating that just by changing the definition of  $(\vec{E}, \vec{H})$  fields, single photon can be described by Maxwell's equations, and therefore, can be simulated using FDTD.

## 2. Time-evolution of TLS

In this part the time-evolution of  $b_i(t)$  coefficient is derived. Our derivation is similar to the procedure provided in [63]. For the considered single-excitation state  $|\Psi(t)\rangle$ , due to the fact that  $b_i = \langle \Psi_G | \hat{\sigma}_i^-(0) | \Psi(t) \rangle + \langle \Psi(t) | \hat{\sigma}_i^-(0) | \Psi_G \rangle$ , the time-derivative is

$$\frac{db_i}{dt} = \frac{d}{dt} \langle \Psi_G | \hat{\sigma}_i^-(0) | \Psi(t) \rangle + \frac{d}{dt} \langle \Psi(t) | \hat{\sigma}_i^-(0) | \Psi_G \rangle. \quad (\text{A15})$$

Transferring between Schrödinger picture and Heisenberg picture leads to

$$\begin{aligned} \langle \Psi_G | \hat{\sigma}^-(0) | \Psi(t) \rangle &= \langle \Psi_G | \exp\left(\frac{i\hat{H}t}{\hbar}\right) \hat{\sigma}^-(0) \exp\left(-\frac{i\hat{H}t}{\hbar}\right) | \Psi(0) \rangle = \langle \Psi_G | \hat{\sigma}^-(t) | \Psi(0) \rangle, \\ \langle \Psi(t) | \hat{\sigma}^-(0) | \Psi_G \rangle &= \langle \Psi(0) | \exp\left(\frac{i\hat{H}t}{\hbar}\right) \hat{\sigma}^-(0) \exp\left(-\frac{i\hat{H}t}{\hbar}\right) | \Psi_G \rangle = \langle \Psi(0) | \hat{\sigma}^-(t) | \Psi_G \rangle. \end{aligned} \quad (\text{A16})$$

Therefore,  $\frac{db_i}{dt}$  can be simplified as

$$\begin{aligned} \frac{db_i}{dt} &= \langle \Psi_G | \frac{d\hat{\sigma}^-(t)}{dt} | \Psi(0) \rangle + \langle \Psi(0) | \frac{d\hat{\sigma}^-(t)}{dt} | \Psi_G \rangle \\ &= -\frac{i}{\hbar} \langle \Psi_G | [\hat{\sigma}^-, \hat{H}] | \Psi(0) \rangle - \frac{i}{\hbar} \langle \Psi(0) | [\hat{\sigma}^-, \hat{H}] | \Psi_G \rangle \\ &= -i\omega_0 \langle \Psi_G | \hat{\sigma}^-(0) | \Psi(t) \rangle - \frac{i}{\hbar} \vec{d}_i \cdot \langle \Psi_G | \hat{\sigma}_z(0) \hat{E}(\vec{r}_i, 0) | \Psi(t) \rangle \\ &\quad - i\omega_0 \langle \Psi(t) | \hat{\sigma}^-(0) | \Psi_G \rangle - \frac{i}{\hbar} \vec{d}_i \cdot \langle \Psi(t) | \hat{E}(\vec{r}_i, 0) \hat{\sigma}_z(0) | \Psi_G \rangle \\ &\quad \underline{\underline{\hat{\sigma}_z = [\hat{\sigma}^+, \hat{\sigma}^-]}} - i\omega_0 b_i + \frac{i}{\hbar} \vec{d}_i \cdot \left( \langle \Psi_G | \hat{E}(\vec{r}_i, 0) | \Psi(t) \rangle + \langle \Psi(t) | \hat{E}(\vec{r}_i, 0) | \Psi_G \rangle \right) \\ &= -i\omega_0 b_i + \frac{i}{\hbar} \vec{d}_i \cdot \vec{E}(\vec{r}_i, t). \end{aligned} \quad (\text{A17})$$

The time-evolution of  $b_i(t)$  coefficient derived here is consistent with the result derived in [63], where the authors focused on single-photon superradiance phenomenon. Still we need to pay attention that the  $\vec{E}(\vec{r}, t)$  field on the right hand side contains the primary radiation. If the primary radiation has been excluded from  $\vec{E}(\vec{r}, t)$ , as is the case in our FDTD algorithm with TF-IF, the spontaneous decay should be included explicitly:

$$\frac{db_i}{dt} = (-i\omega_0 - \frac{\Gamma_{\text{vac}}}{2}) b_i + \frac{i}{\hbar} \vec{d}_i \cdot \vec{E}(\vec{r}_i, t), \quad (\text{A18})$$

arriving at eq. (8) in the main text.

Finally, we provide the derivation of eq. (7) in the main text, ensuring that the oscillating TLS couples back to Maxwell's equations correctly. The  $i$ -th TLS possesses an oscillating dipole moment  $\vec{d}_i(t)$ , which can produce radiation fields. Due to the definition changing of  $\vec{E}(\vec{r}, t)$  and  $\vec{H}(\vec{r}, t)$  fields, the dipole moment should not be calculated as  $\langle \vec{d}_i \rangle = \langle \Psi(t) | \hat{d}_i | \Psi(t) \rangle$ . Instead, it should be calculated as

$$\begin{aligned} \vec{d}_i(t) &= \langle \Psi(t) | \hat{d}_i | \Psi_G \rangle + \langle \Psi_G | \hat{d}_i | \Psi(t) \rangle \\ &= \vec{d}_i \langle \Psi(t) | \hat{\sigma}_i^+ + \hat{\sigma}_i^- | g, 0 \rangle + \vec{d}_i \langle g, 0 | \hat{\sigma}_i^+ + \hat{\sigma}_i^- | \Psi(t) \rangle \\ &= 2\text{Re}(b_i) \cdot \vec{d}_i. \end{aligned} \quad (\text{A19})$$

Therefore, the corresponding current source  $\vec{J}_i(\vec{r})$  used in the  $i$ -th auxiliary FDTD can be derived as

$$\vec{J}_i(\vec{r}) = \frac{d\vec{d}_i(t)}{dt} \delta(\vec{r} - \vec{r}_i) = 2\omega_0 \text{Im}(b_i) \cdot \vec{d}_i \delta(\vec{r} - \vec{r}_i), \quad (\text{A20})$$

which justifies eq. (7) in the main text. Implementing the above expression in 3D FDTD requires us to discretize the Dirac delta function  $\delta(\vec{r} - \vec{r}_i)$ , by replacing it with  $\frac{1}{(\Delta x)^3}$ .

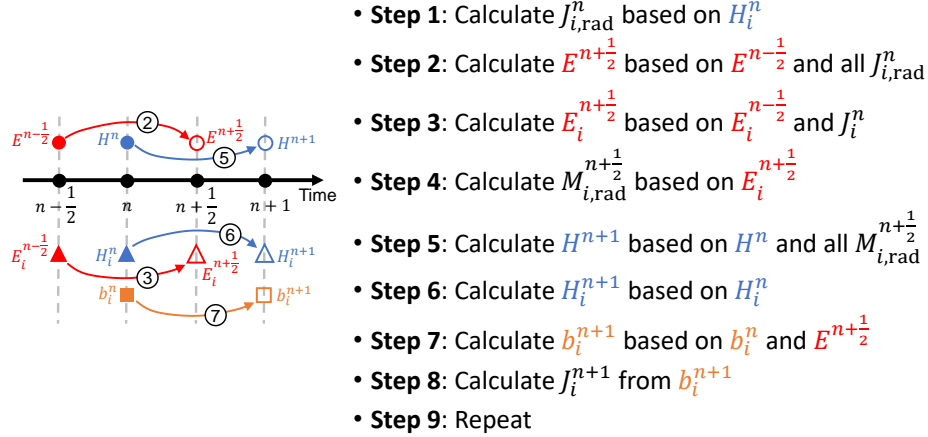


FIG. 5. Procedure of the proposed FDTD. At the  $n$ -th time step, all the electric fields are saved at time  $(n - \frac{1}{2})\Delta t$ , while all the magnetic fields are saved at  $n\Delta t$ . The arrows indicate how the fields are updated. Step 2 and 5 involve only the main FDTD; Step 3 and 6 involve all the auxiliary FDTDs; step 7 and 8 involve the time-evolution of all TLSs.

### Appendix B: General process of proposed FDTD

In this part, the main steps of our proposed FDTD algorithm are summarized. For the sake of simplicity, we mark the fields calculated by the  $i$ -th auxiliary FDTD with footnote  $i$ . For example,  $\vec{H}_i^n$  corresponds to the  $\vec{H}$  field calculated by the  $i$ -th auxiliary FDTD at time  $n\Delta t$ . On the other hand, the fields calculated by the main FDTD do not have footnote.

At the  $n$ -th time step, suppose we have already obtained fields  $\vec{E}^{n-\frac{1}{2}}$  and  $\vec{H}^n$ , as well as  $\vec{E}_i^{n-\frac{1}{2}}$  and  $\vec{H}_i^n$  for all auxiliary FDTDs. The modified FDTD contains the following 9 steps:

- (1) For all  $N$  auxiliary FDTDs: based on  $\vec{H}_i^n$  values on box boundary  $\partial\Omega_i$ , calculate the fictitious current source  $\vec{J}_{i,\text{rad}}^n \sim \hat{n} \times \vec{H}_i^n$ , which will be used in the main FDTD;
- (2) Main FDTD: Calculate  $\vec{E}^{n+\frac{1}{2}}$  based on  $\vec{E}^{n-\frac{1}{2}}$  and all  $\vec{J}_{i,\text{rad}}^n$ 's;
- (3) For all  $N$  auxiliary FDTDs: calculate  $\vec{E}_i^{n+\frac{1}{2}}$  based on  $\vec{E}_i^{n-\frac{1}{2}}$  and  $\vec{J}_i^n$ ;
- (4) For all  $N$  auxiliary FDTDs: based on  $\vec{E}_i^{n+\frac{1}{2}}$  values on box boundary  $\partial\Omega_i$ , calculate the fictitious magnetic current source  $\vec{M}_{i,\text{rad}}^{n+\frac{1}{2}} \sim -\hat{n} \times \vec{E}_i^{n+\frac{1}{2}}$ , which will be used in the main FDTD;
- (5) Main FDTD: Calculate  $\vec{H}^{n+1}$  based on  $\vec{H}^n$  and all  $\vec{M}_{i,\text{rad}}^{n+\frac{1}{2}}$ 's;
- (6) For all  $N$  auxiliary FDTDs: calculate  $\vec{H}_i^{n+1}$  based on  $\vec{H}_i^n$ ;
- (7) For all  $N$  TLSs: update  $b_i^n$  to  $b_i^{n+1}$  based on  $\vec{E}^{n+\frac{1}{2}}(\vec{r}_i)$ ;
- (8) For all  $N$  TLSs: based on coefficient  $b_i^n$ , calculate current sources  $\vec{J}_i^n$ , which will be used in the auxiliary FDTD;
- (9) Repeat the above steps until the stopping criteria is satisfied.

The above procedure is shown schematically in Fig. 5. The implementation details related to 3D FDTD (involving step 2, 3, 5, 6) are provided in Appendix C. The calculation of fictitious current sources  $\vec{J}_{i,\text{rad}}^n$  and  $\vec{M}_{i,\text{rad}}^{n+\frac{1}{2}}$  (involving step 1, 4) is described in Appendix D.

### Appendix C: Implementation details of 3D FDTD

In this part, we provide the details regarding the implementation of FDTD in 3D domain. The contents provided here follow the implementation of a vanilla FDTD, and does not involve any TLS. We start from Maxwell's equations in 3D:

$$\nabla \times \vec{E} = -\frac{\partial \vec{B}}{\partial t} - \vec{M}, \quad (\text{C1})$$

$$\nabla \times \vec{H} = \frac{\partial \vec{D}}{\partial t} + \vec{J}, \quad (\text{C2})$$

which give 6 equations for different field components. More specifically, for  $\vec{H}$  fields:

$$\frac{\partial H_x}{\partial t} = \frac{1}{\mu_{xx}} \left[ \frac{\partial E_y}{\partial z} - \frac{\partial E_z}{\partial y} - (M_x + \sigma_{xx}^* H_x) \right], \quad (\text{C3})$$

$$\frac{\partial H_y}{\partial t} = \frac{1}{\mu_{yy}} \left[ \frac{\partial E_z}{\partial x} - \frac{\partial E_x}{\partial z} - (M_y + \sigma_{yy}^* H_y) \right], \quad (\text{C4})$$

$$\frac{\partial H_z}{\partial t} = \frac{1}{\mu_{zz}} \left[ \frac{\partial E_x}{\partial y} - \frac{\partial E_y}{\partial x} - (M_z + \sigma_{zz}^* H_z) \right]. \quad (\text{C5})$$

For  $\vec{E}$  fields:

$$\frac{\partial E_x}{\partial t} = \frac{1}{\epsilon_{xx}} \left[ \frac{\partial H_z}{\partial y} - \frac{\partial H_y}{\partial z} - (J_x + \sigma_{xx} E_x) \right], \quad (\text{C6})$$

$$\frac{\partial E_y}{\partial t} = \frac{1}{\epsilon_{yy}} \left[ \frac{\partial H_x}{\partial z} - \frac{\partial H_z}{\partial x} - (J_y + \sigma_{yy} E_y) \right], \quad (\text{C7})$$

$$\frac{\partial E_z}{\partial t} = \frac{1}{\epsilon_{zz}} \left[ \frac{\partial H_y}{\partial x} - \frac{\partial H_x}{\partial y} - (J_z + \sigma_{zz} E_z) \right]. \quad (\text{C8})$$

The Yee lattice [1, 98] is defined as shown in Fig. 6, with the same grid size  $\Delta x$  for all three directions  $x$ ,  $y$  and  $z$ . For the sake of simplicity, assume all materials we're working with are uniaxial and non-dispersive. By doing a discretization on Yee lattice, we can derive the update rules (from time step  $n - \frac{1}{2}$  to  $n + \frac{1}{2}$ ) for electric field  $E_x$ ,  $E_y$  and  $E_z$ :

$$E_x^{n+\frac{1}{2}}(i, j, k) = \left( \frac{1 - \frac{\sigma_{xx}\Delta t}{2\epsilon_{xx}}}{1 + \frac{\sigma_{xx}\Delta t}{2\epsilon_{xx}}} \right) E_x^{n-\frac{1}{2}}(i, j, k) + \left( \frac{\frac{\Delta t}{\epsilon_{xx}}}{1 + \frac{\sigma_{xx}\Delta t}{2\epsilon_{xx}}} \right) \cdot \left( \frac{H_z^n(i, j, k) - H_z^n(i, j-1, k)}{\Delta x} - \frac{H_y^n(i, j, k) - H_y^n(i, j, k-1)}{\Delta x} - J_x^n(i, j, k) \right), \quad (\text{C9})$$

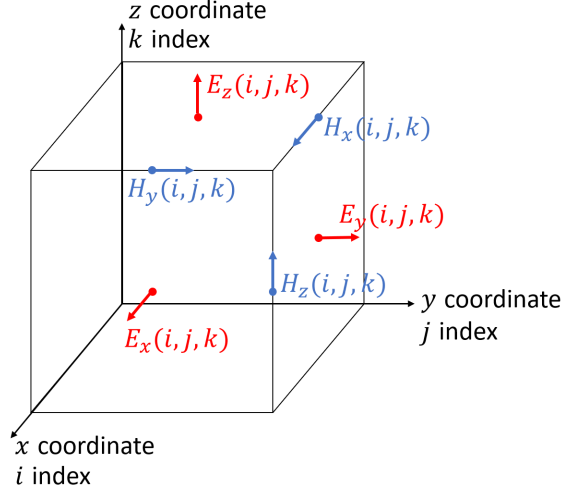


FIG. 6. The Yee lattice used in 3D FDTD. Here only the  $(i, j, k)$  grid point is plotted.

$$E_y^{n+\frac{1}{2}}(i, j, k) = \left( \frac{1 - \frac{\sigma_{yy}\Delta t}{2\epsilon_{yy}}}{1 + \frac{\sigma_{yy}\Delta t}{2\epsilon_{yy}}} \right) E_y^{n-\frac{1}{2}}(i, j, k) + \left( \frac{\frac{\Delta t}{\epsilon_{yy}}}{1 + \frac{\sigma_{yy}\Delta t}{2\epsilon_{yy}}} \right) \cdot \left( \frac{H_x^n(i, j, k) - H_x^n(i, j, k-1)}{\Delta x} - \frac{H_z^n(i, j, k) - H_z^n(i-1, j, k)}{\Delta x} - J_y^n(i, j, k) \right), \quad (\text{C10})$$

$$E_z^{n+\frac{1}{2}}(i, j, k) = \left( \frac{1 - \frac{\sigma_{zz}\Delta t}{2\epsilon_{zz}}}{1 + \frac{\sigma_{zz}\Delta t}{2\epsilon_{zz}}} \right) E_z^{n-\frac{1}{2}}(i, j, k) + \left( \frac{\frac{\Delta t}{\epsilon_{zz}}}{1 + \frac{\sigma_{zz}\Delta t}{2\epsilon_{zz}}} \right) \cdot \left( \frac{H_y^n(i, j, k) - H_y^n(i-1, j, k)}{\Delta x} - \frac{H_x^n(i, j, k) - H_x^n(i, j-1, k)}{\Delta x} - J_z^n(i, j, k) \right). \quad (\text{C11})$$

Similarly, the update rules for magnetic field  $H_x$ ,  $H_y$  and  $H_z$  (from time step  $n$  to  $n+1$ ) are:

$$H_x^{n+1}(i, j, k) = \left( \frac{1 - \frac{\sigma_{xx}^*\Delta t}{2\mu_{xx}}}{1 + \frac{\sigma_{xx}^*\Delta t}{2\mu_{xx}}} \right) H_x^n(i, j, k) + \left( \frac{\frac{\Delta t}{\mu_{xx}}}{1 + \frac{\sigma_{xx}^*\Delta t}{2\mu_{xx}}} \right) \cdot \left( \frac{E_y^{n+\frac{1}{2}}(i, j, k+1) - E_y^{n+\frac{1}{2}}(i, j, k)}{\Delta x} - \frac{E_z^{n+\frac{1}{2}}(i, j+1, k) - E_z^{n+\frac{1}{2}}(i, j, k)}{\Delta x} - M_x^{n+\frac{1}{2}}(i, j, k) \right), \quad (\text{C12})$$

$$H_y^{n+1}(i, j, k) = \left( \frac{1 - \frac{\sigma_{yy}^*\Delta t}{2\mu_{yy}}}{1 + \frac{\sigma_{yy}^*\Delta t}{2\mu_{yy}}} \right) H_y^n(i, j, k) + \left( \frac{\frac{\Delta t}{\mu_{yy}}}{1 + \frac{\sigma_{yy}^*\Delta t}{2\mu_{yy}}} \right) \cdot \left( \frac{E_z^{n+\frac{1}{2}}(i+1, j, k) - E_z^{n+\frac{1}{2}}(i, j, k)}{\Delta x} - \frac{E_x^{n+\frac{1}{2}}(i, j, k+1) - E_x^{n+\frac{1}{2}}(i, j, k)}{\Delta x} - M_y^{n+\frac{1}{2}}(i, j, k) \right), \quad (\text{C13})$$

$$\begin{aligned}
H_z^{n+1}(i, j, k) &= \left( \frac{1 - \frac{\sigma_{zz}^* \Delta t}{2\mu_{zz}}}{1 + \frac{\sigma_{zz}^* \Delta t}{2\mu_{zz}}} \right) H_z^n(i, j, k) + \left( \frac{\frac{\Delta t}{\mu_{zz}}}{1 + \frac{\sigma_{zz}^* \Delta t}{2\mu_{zz}}} \right) \\
&\cdot \left( \frac{E_x^{n+\frac{1}{2}}(i, j+1, k) - E_x^{n+\frac{1}{2}}(i, j, k)}{\Delta x} - \frac{E_y^{n+\frac{1}{2}}(i+1, j, k) - E_y^{n+\frac{1}{2}}(i, j, k)}{\Delta x} - M_z^{n+\frac{1}{2}}(i, j, k) \right). \tag{C14}
\end{aligned}$$

The above 6 equations form the update rule of vanilla FDTD simulation in 3D domain.

#### Appendix D: Implementation details of TF-IF technique

In this part, the implementation of step 1 (and 4) is introduced in detail. We focus on the  $i$ -th TLS and present the relationship between the fictitious current sources  $(\vec{J}_{i,\text{rad}}, \vec{M}_{i,\text{rad}})$  and the fields  $(\vec{E}_{i,\text{rad}}, \vec{H}_{i,\text{rad}})$  calculated by the  $i$ -th auxiliary FDTD. For the sake of simplicity, assume that a square box is selected as region  $\Omega_i$ , which is the case for all FDTD simulations presented in this paper. The square box spans  $[i_1, i_2]$  in  $x$  direction,  $[j_1, j_2]$  in  $y$  direction, and  $[k_1, k_2]$  in  $z$  direction. The TLS is located at the center of box  $\Omega_i$ .

At each time step, after the primary radiation fields  $(\vec{E}_{i,\text{rad}}, \vec{H}_{i,\text{rad}})$  have been calculated in the  $i$ -th auxiliary FDTD, we'd like to excite the exact same radiation fields outside  $\Omega_i$  in the main FDTD. To achieve this, these field values  $(\vec{E}_{i,\text{rad}}, \vec{H}_{i,\text{rad}})$  have to be converted into fictitious surface current densities. Based on the surface equivalence principle, we need to place surface current density  $\hat{n} \times \vec{H}_i$  as well as surface magnetic current density  $-\hat{n} \times \vec{E}_i$  on  $\partial\Omega_i$ . It's straightforward to figure out the required surface current densities on all region boundaries (here we ignore the "rad" footnote for simplicity, while including a "surf" footnote to indicate that these are surface current densities):

$$\begin{aligned}
i = i_1, \hat{n} = (-1, 0, 0) : \vec{J}_{i,\text{surf}} &= (0, H_{i,z}, -H_{i,y}), \vec{M}_{i,\text{surf}} = (0, -E_{i,z}, E_{i,y}); \\
i = i_2, \hat{n} = (1, 0, 0) : \vec{J}_{i,\text{surf}} &= (0, -H_{i,z}, H_{i,y}), \vec{M}_{i,\text{surf}} = (0, E_{i,z}, -E_{i,y}); \tag{D1}
\end{aligned}$$

$$\begin{aligned}
j = j_1, \hat{n} = (0, -1, 0) : \vec{J}_{i,\text{surf}} &= (-H_{i,z}, 0, H_{i,x}), \vec{M}_{i,\text{surf}} = (E_{i,z}, 0, -E_{i,x}); \\
j = j_2, \hat{n} = (0, 1, 0) : \vec{J}_{i,\text{surf}} &= (H_{i,z}, 0, -H_{i,x}), \vec{M}_{i,\text{surf}} = (-E_{i,z}, 0, E_{i,x}); \tag{D2}
\end{aligned}$$

$$\begin{aligned}
k = k_1, \hat{n} = (0, 0, -1) : \vec{J}_{i,\text{surf}} &= (H_{i,y}, -H_{i,x}, 0), \vec{M}_{i,\text{surf}} = (-E_{i,y}, E_{i,x}, 0); \\
k = k_2, \hat{n} = (0, 0, 1) : \vec{J}_{i,\text{surf}} &= (-H_{i,y}, H_{i,x}, 0), \vec{M}_{i,\text{surf}} = (E_{i,y}, -E_{i,x}, 0). \tag{D3}
\end{aligned}$$

The above surface current densities need to be discretized before being introduced into the main FDTD. More specifically, in order to add  $\vec{J}_{i,\text{surf}}$  and  $\vec{M}_{i,\text{surf}}$  into the main FDTD at the  $n$ -th time step, the current sources at the following grid points are modified:

(1)  $i = i_1$ :

$$\begin{aligned}
J_y^n(i_1, j, k) &= \frac{H_{i,z}^n(i_1 - 1, j, k)}{\Delta x}, & \text{for } j = j_1, \dots, j_2 - 1 \text{ and } k = k_1, \dots, k_2; \\
J_z^n(i_1, j, k) &= \frac{-H_{i,y}^n(i_1 - 1, j, k)}{\Delta x}, & \text{for } j = j_1, \dots, j_2 \text{ and } k = k_1, \dots, k_2 - 1; \\
M_y^{n+\frac{1}{2}}(i_1 - 1, j, k) &= \frac{-E_{i,z}^{n+\frac{1}{2}}(i_1, j, k)}{\Delta x}, & \text{for } j = j_1, \dots, j_2 \text{ and } k = k_1, \dots, k_2 - 1; \\
M_z^{n+\frac{1}{2}}(i_1 - 1, j, k) &= \frac{E_{i,y}^{n+\frac{1}{2}}(i_1, j, k)}{\Delta x}, & \text{for } j = j_1, \dots, j_2 - 1 \text{ and } k = k_1, \dots, k_2.
\end{aligned} \tag{D4}$$

(2)  $i = i_2$ :

$$\begin{aligned}
J_y^n(i_2, j, k) &= \frac{-H_{i,z}^n(i_2, j, k)}{\Delta x}, & \text{for } j = j_1, \dots, j_2 - 1 \text{ and } k = k_1, \dots, k_2; \\
J_z^n(i_2, j, k) &= \frac{H_{i,y}^n(i_2, j, k)}{\Delta x}, & \text{for } j = j_1, \dots, j_2 \text{ and } k = k_1, \dots, k_2 - 1; \\
M_y^{n+\frac{1}{2}}(i_2, j, k) &= \frac{E_{i,z}^{n+\frac{1}{2}}(i_2, j, k)}{\Delta x}, & \text{for } j = j_1, \dots, j_2 \text{ and } k = k_1, \dots, k_2 - 1; \\
M_z^{n+\frac{1}{2}}(i_2, j, k) &= \frac{-E_{i,y}^{n+\frac{1}{2}}(i_2, j, k)}{\Delta x}, & \text{for } j = j_1, \dots, j_2 - 1 \text{ and } k = k_1, \dots, k_2.
\end{aligned} \tag{D5}$$

(3)  $j = j_1$ :

$$\begin{aligned}
J_x^n(i, j_1, k) &= \frac{-H_{i,z}^n(i, j_1 - 1, k)}{\Delta x}, & \text{for } i = i_1, \dots, i_2 - 1 \text{ and } k = k_1, \dots, k_2; \\
J_z^n(i, j_1, k) &= \frac{H_{i,x}^n(i, j_1 - 1, k)}{\Delta x}, & \text{for } i = i_1, \dots, i_2 \text{ and } k = k_1, \dots, k_2 - 1; \\
M_x^{n+\frac{1}{2}}(i, j_1 - 1, k) &= \frac{E_{i,z}^{n+\frac{1}{2}}(i, j_1, k)}{\Delta x}, & \text{for } i = i_1, \dots, i_2 \text{ and } k = k_1, \dots, k_2 - 1; \\
M_z^{n+\frac{1}{2}}(i, j_1 - 1, k) &= \frac{-E_{i,x}^{n+\frac{1}{2}}(i, j_1, k)}{\Delta x}, & \text{for } i = i_1, \dots, i_2 - 1 \text{ and } k = k_1, \dots, k_2.
\end{aligned} \tag{D6}$$

(4)  $j = j_2$ :

$$\begin{aligned}
J_x^n(i, j_2, k) &= \frac{H_{i,z}^n(i, j_2, k)}{\Delta x}, & \text{for } i = i_1, \dots, i_2 - 1 \text{ and } k = k_1, \dots, k_2; \\
J_z^n(i, j_2, k) &= \frac{-H_{i,x}^n(i, j_2, k)}{\Delta x}, & \text{for } i = i_1, \dots, i_2 \text{ and } k = k_1, \dots, k_2 - 1; \\
M_x^{n+\frac{1}{2}}(i, j_2, k) &= \frac{-E_{i,z}^{n+\frac{1}{2}}(i, j_2, k)}{\Delta x}, & \text{for } i = i_1, \dots, i_2 \text{ and } k = k_1, \dots, k_2 - 1; \\
M_z^{n+\frac{1}{2}}(i, j_2, k) &= \frac{E_{i,x}^{n+\frac{1}{2}}(i, j_2, k)}{\Delta x}, & \text{for } i = i_1, \dots, i_2 - 1 \text{ and } k = k_1, \dots, k_2.
\end{aligned} \tag{D7}$$



(5)  $k = k_1$ :

$$\begin{aligned}
J_x^n(i, j, k_1) &= \frac{H_{i,y}^n(i, j, k_1 - 1)}{\Delta x}, & \text{for } i = i_1, \dots, i_2 - 1 \text{ and } j = j_1, \dots, j_2; \\
J_y^n(i, j, k_1) &= \frac{-H_{i,x}^n(i, j, k_1 - 1)}{\Delta x}, & \text{for } i = i_1, \dots, i_2 \text{ and } j = j_1, \dots, j_2 - 1; \\
M_x^{n+\frac{1}{2}}(i, j, k_1 - 1) &= \frac{-E_{i,y}^{n+\frac{1}{2}}(i, j, k_1)}{\Delta x}, & \text{for } i = i_1, \dots, i_2 \text{ and } j = j_1, \dots, j_2 - 1; \\
M_y^{n+\frac{1}{2}}(i, j, k_1 - 1) &= \frac{E_{i,x}^{n+\frac{1}{2}}(i, j, k_1)}{\Delta x}, & \text{for } i = i_1, \dots, i_2 - 1 \text{ and } j = j_1, \dots, j_2.
\end{aligned} \tag{D8}$$

(6)  $k = k_2$ :

$$\begin{aligned}
J_x^n(i, j, k_2) &= \frac{-H_{i,y}^n(i, j, k_2)}{\Delta x}, & \text{for } i = i_1, \dots, i_2 - 1 \text{ and } j = j_1, \dots, j_2; \\
J_y^n(i, j, k_2) &= \frac{H_{i,x}^n(i, j, k_2)}{\Delta x}, & \text{for } i = i_1, \dots, i_2 \text{ and } j = j_1, \dots, j_2 - 1; \\
M_x^{n+\frac{1}{2}}(i, j, k_2) &= \frac{E_{i,y}^{n+\frac{1}{2}}(i, j, k_2)}{\Delta x}, & \text{for } i = i_1, \dots, i_2 \text{ and } j = j_1, \dots, j_2 - 1; \\
M_y^{n+\frac{1}{2}}(i, j, k_2) &= \frac{-E_{i,x}^{n+\frac{1}{2}}(i, j, k_2)}{\Delta x}, & \text{for } i = i_1, \dots, i_2 - 1 \text{ and } j = j_1, \dots, j_2.
\end{aligned} \tag{D9}$$

Following the above six equations, by introducing the current sources into the main FDTD, the  $i$ -th TLS's radiation fields will only be excited outside region  $\Omega_i$ . Our method is similar to the one proposed in [32]. However there's a key difference between our TF-IF implementation and the method used in [32]: instead of using an analytical expression of dipole radiation, here the radiation fields are calculated numerically. This leads to improved accuracy, enabling us to shrink the size of IF region  $\Omega_i$  down to  $3 \times 3 \times 3$  grid points. As a comparison, in [32] the authors used a box that's larger than  $7 \times 7 \times 7$  grid points. Thanks to this, we have been able to simulate cases where multiple TLSs are placed very close to each other (as close as  $2\Delta x$ ), as shown in the main text.

The computational overhead of the auxiliary FDTDs is small compared to the computational cost of main FDTD. For example, in the cavity QED simulation, the simulation domain of main FDTD contains  $240 \times 254 \times 90 \approx 5.49$  million grid points. Each auxiliary FDTD, on the other hand, contains  $55^3 \approx 0.16$  million grid points. This makes it possible to incorporate a few TLSs into FDTD simulation without significantly increasing the simulation time.

### Appendix E: Numerical solver for TLS's dynamics

In this part, the implementation of step 7 is introduced in detail. The differential equations used for 2 baseline semi-classical methods are also provided.

For the  $i$ -th TLS located at position  $\vec{r}_i$ , we first sample the electric field  $\vec{E}^{n+\frac{1}{2}}(\vec{r}_i)$  at its location from the main FDTD. This value is then utilized to drive the TLS, by doing a time-marching of the following equation:

$$\frac{db_i}{dt} = (-i\omega_0 - \frac{\Gamma_{\text{vac}}}{2})b_i + \frac{i}{\hbar}\vec{d}_i \cdot \vec{E}(\vec{r}_i, t), \quad (\text{E1})$$

where  $\Gamma_{\text{vac}}$  stands for the TLS's spontaneous decay rate inside vacuum. This decay term is included due to the fact that the primary radiation field has been excluded in  $\vec{E}^{n+\frac{1}{2}}(\vec{r}_i)$ .

As for Maxwell-Schrödinger equations, the quantum state of the  $i$ -th TLS can be represented using 2 coefficients:  $|\Psi_i(t)\rangle = c_{i,g}(t)|g\rangle + c_{i,e}(t)|e\rangle$ . The time-evolution of these coefficients follow

$$\begin{aligned} \frac{\partial c_{i,e}}{\partial t} &= -i\omega_0 c_{i,e} + \frac{i}{\hbar}\vec{d}_i \cdot \vec{E}(\vec{r}_i, t)c_{i,g}, \\ \frac{\partial c_{i,g}}{\partial t} &= \frac{i}{\hbar}\vec{d}_i \cdot \vec{E}(\vec{r}_i, t)c_{i,e}. \end{aligned} \quad (\text{E2})$$

By looking at the above equations, we can notice that if a single TLS starts from excited state with  $c_{i,g}(t=0) = 0$ , its coherence  $c_{i,e}^*c_{i,g}$  will remain zero for  $t > 0$ , therefore cannot produce nonzero field.

On the other hand, for Maxwell-Bloch equations, the time-evolution of the  $i$ -th TLS involves elements of density matrix  $\hat{\rho}_i$ :

$$\begin{aligned} \frac{\partial \rho_{i,ee}}{\partial t} &= \frac{i}{\hbar}\vec{d}_i \cdot \vec{E}(\vec{r}_i, t) \cdot (\rho_{i,eg}^* - \rho_{i,eg}) - \Gamma_{\text{vac}}\rho_{i,ee}, \\ \frac{\partial \rho_{i,eg}}{\partial t} &= (-i\omega_0 - \frac{\Gamma_{\text{vac}}}{2})\rho_{i,eg} + \frac{i}{\hbar}\vec{d}_i \cdot \vec{E}(\vec{r}_i, t) \cdot (1 - 2\rho_{i,ee}). \end{aligned} \quad (\text{E3})$$

Similarly, if a single TLS starts from excited state with  $\rho_{i,eg}(t=0) = 0$ , its coherence  $\rho_{i,eg}$  will remain zero for  $t > 0$ . Even though the population  $\rho_{i,ee}$  decays exponentially, no electromagnetic fields can be excited when using semi-classical simulation techniques.

The above sets of equations can be solved using any type of differential equation solver. In this paper, instead of using Euler method (which often leads to divergence), we apply the 4-th order Runge-Kutta method, with a time step of  $\Delta t/5$  to ensure accuracy.

- 
- [1] A. Taflove, S. C. Hagness, and M. Piket-May, Computational electromagnetics: the finite-difference time-domain method, The Electrical Engineering Handbook **3**, 15 (2005).  
 [2] Tidy3d solver, <https://www.flexcompute.com/tidy3d/solver/>, accessed: 2024-05-19.

- [3] A. F. Oskooi, D. Roundy, M. Ibanescu, P. Bermel, J. D. Joannopoulos, and S. G. Johnson, Meep: A flexible free-software package for electromagnetic simulations by the ftdtd method, Computer Physics Communications **181**, 687 (2010).

- [4] A. Javadi, I. Söllner, M. Arcari, S. L. Hansen, L. Midolo, S. Mahmoodian, G. Kiršanskė, T. Pognolato, E. Lee, J. Song, *et al.*, Single-photon non-linear optics with a quantum dot in a waveguide, *Nature communications* **6**, 8655 (2015).
- [5] D. E. Chang, V. Vuletić, and M. D. Lukin, Quantum nonlinear optics—photon by photon, *Nature Photonics* **8**, 685 (2014).
- [6] R. F. Ribeiro, L. A. Martínez-Martínez, M. Du, J. Campos-Gonzalez-Angulo, and J. Yuen-Zhou, Polariton chemistry: controlling molecular dynamics with optical cavities, *Chemical science* **9**, 6325 (2018).
- [7] A. Mandal, M. A. Taylor, B. M. Weight, E. R. Koessler, X. Li, and P. Huo, Theoretical advances in polariton chemistry and molecular cavity quantum electrodynamics, *Chemical Reviews* **123**, 9786 (2023).
- [8] S. K. Biswas, W. Adi, A. Beisenova, S. Rosas, E. R. Arvelo, and F. Yesilkoy, From weak to strong coupling: quasi-bic metasurfaces for mid-infrared light–matter interactions, *Nanophotonics* doi:10.1515/nanoph-2024-0043 (2024).
- [9] A. Asenjo-Garcia, M. Moreno-Cardoner, A. Albrecht, H. Kimble, and D. E. Chang, Exponential improvement in photon storage fidelities using subradiance and “selective radiance” in atomic arrays, *Physical Review X* **7**, 031024 (2017).
- [10] X.-W. Chen, V. Sandoghdar, and M. Agio, Coherent interaction of light with a metallic structure coupled to a single quantum emitter: from superabsorption to cloaking, *Physical review letters* **110**, 153605 (2013).
- [11] A. S. Sheremet, M. I. Petrov, I. V. Iorsh, A. V. Poshakinskiy, and A. N. Poddubny, Waveguide quantum electrodynamics: collective radiance and photon-photon correlations, *Reviews of Modern Physics* **95**, 015002 (2023).
- [12] D. Englund, D. Fattal, E. Waks, G. Solomon, B. Zhang, T. Nakaoka, Y. Arakawa, Y. Yamamoto, and J. Vučković, Controlling the spontaneous emission rate of single quantum dots in a two-dimensional photonic crystal, *Phys. Rev. Lett.* **95**, 013904 (2005).
- [13] L. Ying, M. Zhou, M. Mattei, B. Liu, P. Campagnola, R. H. Goldsmith, and Z. Yu, Extended range of dipole-dipole interactions in periodically structured photonic media, *Physical Review Letters* **123**, 173901 (2019).
- [14] M. Scheucher, A. Hilico, E. Will, J. Volz, and A. Rauschenbeutel, Quantum optical circulator controlled by a single chirally coupled atom, *Science* **354**, 1577 (2016).
- [15] C. L. Cortes and Z. Jacob, Super-coulombic atom–atom interactions in hyperbolic media, *Nature communications* **8**, 14144 (2017).
- [16] A. Sipahigil, R. E. Evans, D. D. Sukachev, M. J. Burek, J. Borregaard, M. K. Bhaskar, C. T. Nguyen, J. L. Pacheco, H. A. Atikian, C. Meuwly, *et al.*, An integrated diamond nanophotonics platform for quantum-optical networks, *Science* **354**, 847 (2016).
- [17] M. Zhao and K. Fang, Photon-photon interaction mediated by a virtual photon in a nonlinear microcavity, arXiv preprint arXiv:2304.11676 (2023).
- [18] E. T. Jaynes and F. W. Cummings, Comparison of quantum and semiclassical radiation theories with application to the beam maser, *Proceedings of the IEEE* **51**, 89 (1963).
- [19] M. Tavis and F. W. Cummings, Exact solution for an n-molecule—radiation-field hamiltonian, *Physical Review* **170**, 379 (1968).
- [20] D. Wang, Cavity quantum electrodynamics with a single molecule: Purcell enhancement, strong coupling and single-photon nonlinearity, *Journal of Physics B: Atomic, Molecular and Optical Physics* **54**, 133001 (2021).
- [21] J.-t. Shen and S. Fan, Coherent photon transport from spontaneous emission in one-dimensional waveguides, *Optics letters* **30**, 2001 (2005).
- [22] S. Fan, Ş. E. Kocabaş, and J.-T. Shen, Input-output formalism for few-photon transport in one-dimensional nanophotonic waveguides coupled to a qubit, *Physical Review A* **82**, 063821 (2010).
- [23] Z. Ficek and S. Swain, *Quantum interference and coherence: theory and experiments*, Vol. 100 (Springer Science & Business Media, 2005).
- [24] A. Asenjo-Garcia, J. Hood, D. Chang, and H. Kimble, Atom-light interactions in quasi-one-dimensional nanostructures: A green’s-function perspective, *Physical Review A* **95**, 033818 (2017).
- [25] P. Meystre and M. Sargent, *Elements of quantum optics* (Springer Science & Business Media, 2007).
- [26] R. W. Ziolkowski, J. M. Arnold, and D. M. Gogny, Ultrafast pulse interactions with two-level atoms, *Physical Review A* **52**, 3082 (1995).

- [27] M. Riesch and C. Jirauschek, mbsolve: An open-source solver tool for the maxwell-bloch equations, *Computer Physics Communications* **268**, 108097 (2021).
- [28] Y. P. Chen, E. Wei, L. Jiang, M. Meng, Y. M. Wu, and W. C. Chew, A unified hamiltonian solution to maxwell-schrödinger equations for modeling electromagnetic field-particle interaction, *Computer physics communications* **215**, 63 (2017).
- [29] T. Takeuchi, S. Ohnuki, and T. Sako, Maxwell-schrödinger hybrid simulation for optically controlling quantum states: A scheme for designing control pulses, *Physical Review A* **91**, 033401 (2015).
- [30] K. Lopata and D. Neuhauser, Multiscale maxwell-schrödinger modeling: A split field finite-difference time-domain approach to molecular nanopolaritons, *The Journal of chemical physics* **130** (2009).
- [31] T. E. Li, H.-T. Chen, and J. E. Subotnik, Comparison of different classical, semiclassical, and quantum treatments of light-matter interactions: Understanding energy conservation, *Journal of Chemical Theory and Computation* **15**, 1957 (2019).
- [32] A. Deinega and T. Seideman, Self-interaction-free approaches for self-consistent solution of the maxwell-liouville equations, *Physical Review A* **89**, 022501 (2014).
- [33] E. Schelew, R.-C. Ge, S. Hughes, J. Pond, and J. F. Young, Self-consistent numerical modeling of radiatively damped lorentz oscillators, *Physical Review A* **95**, 063853 (2017).
- [34] P. W. Milonni and P. L. Knight, Retardation in the resonant interaction of two identical atoms, *Physical Review A* **10**, 1096 (1974).
- [35] K. H. Madsen, S. Ates, T. Lund-Hansen, A. Löffler, S. Reitzenstein, A. Forchel, and P. Lodahl, Observation of non-markovian dynamics of a single quantum dot in a micropillar cavity, *Physical review letters* **106**, 233601 (2011).
- [36] M. Cheneau, P. Barmettler, D. Poletti, M. Endres, P. Schauß, T. Fukuhara, C. Gross, I. Bloch, C. Kollath, and S. Kuhr, Light-cone-like spreading of correlations in a quantum many-body system, *Nature* **481**, 484 (2012).
- [37] D. O. Krimer, M. Liertzer, S. Rotter, and H. E. Türeci, Route from spontaneous decay to complex multimode dynamics in cavity qed, *Physical Review A* **89**, 033820 (2014).
- [38] N. M. Sundaresan, Y. Liu, D. Sadri, L. J. Szócs, D. L. Underwood, M. Malekakhlagh, H. E. Türeci, and A. A. Houck, Beyond strong coupling in a multimode cavity, *Physical Review X* **5**, 021035 (2015).
- [39] D. Lentrodt, O. Diekmann, C. H. Keitel, S. Rotter, and J. Evers, Certifying multimode light-matter interaction in lossy resonators, *Physical Review Letters* **130**, 263602 (2023).
- [40] T. S. Haugland, C. Schäfer, E. Ronca, A. Rubio, and H. Koch, Intermolecular interactions in optical cavities: An ab initio qed study, *The Journal of Chemical Physics* **154** (2021).
- [41] E. Yablonovitch, Inhibited spontaneous emission in solid-state physics and electronics, *Physical review letters* **58**, 2059 (1987).
- [42] S.-P. Yu, J. A. Muniz, C.-L. Hung, and H. Kimble, Two-dimensional photonic crystals for engineering atom-light interactions, *Proceedings of the National Academy of Sciences* **116**, 12743 (2019).
- [43] J. Perczel and M. D. Lukin, Theory of dipole radiation near a dirac photonic crystal, *Physical Review A* **101**, 033822 (2020).
- [44] Y.-G. Huang, G. Chen, C.-J. Jin, W. Liu, and X.-H. Wang, Dipole-dipole interaction in a photonic crystal nanocavity, *Physical Review A* **85**, 053827 (2012).
- [45] A. González-Tudela and J. I. Cirac, Exotic quantum dynamics and purely long-range coherent interactions in dirac conelike baths, *Physical Review A* **97**, 043831 (2018).
- [46] B. Bidégaray, Time discretizations for maxwell-bloch equations, *Numerical Methods for Partial Differential Equations: An International Journal* **19**, 284 (2003).
- [47] J. A. Gruetzmacher and N. F. Scherer, Finite-difference time-domain simulation of ultrashort pulse propagation incorporating quantum-mechanical response functions, *Optics letters* **28**, 573 (2003).
- [48] K. Lopata and D. Neuhauser, Nonlinear nanopolaritons: Finite-difference time-domain maxwell-schrödinger simulation of molecule-assisted plasmon transfer, *The Journal of chemical physics* **131** (2009).
- [49] H. Taniyama, H. Sumikura, and M. Notomi, Finite-difference time-domain analysis of photonic crystal slab cavities with two-level systems, *Optics Express* **19**, 23067 (2011).
- [50] C. J. Ryu, A. Y. Liu, E. Wei, and W. C. Chew, Finite-difference time-domain simulation of the maxwell-schrödinger system, *IEEE Journal on Multiscale and Multiphysics Com-*

- putational Techniques **1**, 40 (2016).
- [51] W. Cartar, J. Mørk, and S. Hughes, Self-consistent maxwell-bloch model of quantum-dot photonic-crystal-cavity lasers, *Physical Review A* **96**, 023859 (2017).
- [52] J. Olthaus, M. Sohr, S. Wong, S. S. Oh, and D. E. Reiter, Modeling spatiotemporal dynamics of chiral coupling of quantum emitters to light fields in nanophotonic structures, *Physical Review A* **107**, 023502 (2023).
- [53] H. A. Bethe, The electromagnetic shift of energy levels, *Physical Review* **72**, 339 (1947).
- [54] D. A. Steck, *Quantum and atom optics* (Self-published, 2007).
- [55] G. Zumofen, N. Mojarad, V. Sandoghdar, and M. Agio, Perfect reflection of light by an oscillating dipole, *Physical Review Letters* **101**, 180404 (2008).
- [56] J. Liu, M. Zhou, and Z. Yu, Quantum scattering theory of a single-photon fock state in three-dimensional spaces, *Optics letters* **41**, 4166 (2016).
- [57] M. Zhou, L. Shi, J. Zi, and Z. Yu, Extraordinarily large optical cross section for localized single nanoresonator, *Physical review letters* **115**, 023903 (2015).
- [58] J. Liu, M. Zhou, L. Ying, X. Chen, and Z. Yu, Enhancing the optical cross section of quantum antenna, *Physical Review A* **95**, 013814 (2017).
- [59] S. Tretyakov, Maximizing absorption and scattering by dipole particles, *Plasmonics* **9**, 935 (2014).
- [60] R. W. Boyd, A. L. Gaeta, and E. Giese, Non-linear optics, in *Springer Handbook of Atomic, Molecular, and Optical Physics* (Springer, 2008) pp. 1097–1110.
- [61] J.-M. Jin, *Theory and computation of electromagnetic fields* (John Wiley & Sons, 2015).
- [62] T. E. Li, H.-T. Chen, A. Nitzan, M. Sukharev, and J. E. Subotnik, A necessary trade-off for semiclassical electrodynamics: accurate short-range coulomb interactions versus the enforcement of causality?, *The Journal of Physical Chemistry Letters* **9**, 5955 (2018).
- [63] A. A. Svidzinsky, X. Zhang, and M. O. Scully, Quantum versus semiclassical description of light interaction with atomic ensembles: Revision of the maxwell-bloch equations and single-photon superradiance, *Physical Review A* **92**, 013801 (2015).
- [64] M. O. Scully, Collective lamb shift in single photon dicke superradiance, *Physical review letters* **102**, 143601 (2009).
- [65] H. T. Dung, L. Knöll, and D.-G. Welsch, Resonant dipole-dipole interaction in the presence of dispersing and absorbing surroundings, *Physical Review A* **66**, 063810 (2002).
- [66] L. Ying, M. S. Mattei, B. Liu, S.-Y. Zhu, R. H. Goldsmith, and Z. Yu, Strong and long-range radiative interaction between resonant transitions, *Physical Review Research* **4**, 013118 (2022).
- [67] S. A. Hassani Gangaraj, L. Ying, F. Monticone, and Z. Yu, Enhancement of quantum excitation transport by photonic nonreciprocity, *Physical Review A* **106**, 033501 (2022).
- [68] M. O. Scully, E. S. Fry, C. R. Ooi, and K. Wódkiewicz, Directed spontaneous emission from an extended ensemble of n atoms: Timing is everything, *Physical review letters* **96**, 010501 (2006).
- [69] H.-T. Chen, T. E. Li, M. Sukharev, A. Nitzan, and J. E. Subotnik, Ehrenfest+ r dynamics. i. a mixed quantum-classical electrodynamics simulation of spontaneous emission, *The Journal of chemical physics* **150** (2019).
- [70] T. E. Li, A. Nitzan, M. Sukharev, T. Martinez, H.-T. Chen, and J. E. Subotnik, Mixed quantum-classical electrodynamics: Understanding spontaneous decay and zero-point energy, *Physical Review A* **97**, 032105 (2018).
- [71] G. A. Jones and D. S. Bradshaw, Resonance energy transfer: from fundamental theory to recent applications, *Frontiers in Physics* **7**, 100 (2019).
- [72] D. L. Andrews and D. S. Bradshaw, Virtual photons, dipole fields and energy transfer: a quantum electrodynamical approach, *European journal of physics* **25**, 845 (2004).
- [73] S. Ravets, H. Labuhn, D. Barredo, L. Béguin, T. Lahaye, and A. Browaeys, Coherent dipole-dipole coupling between two single rydberg atoms at an electrically-tuned förster resonance, *Nature Physics* **10**, 914 (2014).
- [74] M. Şener, J. Strümpfer, J. Hsin, D. Chandler, S. Scheuring, C. N. Hunter, and K. Schulten, Förster energy transfer theory as reflected in the structures of photosynthetic light-harvesting systems, *ChemPhysChem* **12**, 518 (2011).
- [75] G. D. Scholes, Long-range resonance energy transfer in molecular systems, *Annual review of physical chemistry* **54**, 57 (2003).
- [76] N. Hildebrandt, C. M. Spillmann, W. R. Algar, T. Pons, M. H. Stewart, E. Oh,

- K. Susumu, S. A. Diaz, J. B. Delehanty, and I. L. Medintz, Energy transfer with semiconductor quantum dot bioconjugates: a versatile platform for biosensing, energy harvesting, and other developing applications, *Chemical reviews* **117**, 536 (2017).
- [77] W. R. Algar, N. Hildebrandt, S. S. Vogel, and I. L. Medintz, FRET as a biomolecular research tool—understanding its potential while avoiding pitfalls, *Nature methods* **16**, 815 (2019).
- [78] E. Goldstein and P. Meystre, Dipole-dipole interaction in optical cavities, *Physical Review A* **56**, 5135 (1997).
- [79] A. Cerjan, A. Oskooi, S.-L. Chua, and S. G. Johnson, Modeling lasers and saturable absorbers via multilevel atomic media in the meep fdtd software: Theory and implementation, arXiv preprint arXiv:2007.09329 (2020).
- [80] S. J. Masson and A. Asenjo-Garcia, Universality of Dicke superradiance in arrays of quantum emitters, *Nature Communications* **13**, 2285 (2022).
- [81] S. J. Masson, I. Ferrier-Barbut, L. A. Orozco, A. Browaeys, and A. Asenjo-Garcia, Many-body signatures of collective decay in atomic chains, *Physical review letters* **125**, 263601 (2020).
- [82] M. O. Scully and A. A. Svidzinsky, The super of superradiance, *Science* **325**, 1510 (2009).
- [83] M. Gross and S. Haroche, Superradiance: An essay on the theory of collective spontaneous emission, *Physics reports* **93**, 301 (1982).
- [84] R. H. Dicke, Coherence in spontaneous radiation processes, *Physical review* **93**, 99 (1954).
- [85] J. A. Mlynek, A. A. Abdumalikov, C. Eichler, and A. Wallraff, Observation of Dicke superradiance for two artificial atoms in a cavity with high decay rate, *Nature communications* **5**, 5186 (2014).
- [86] J.-B. Trebbia, Q. Deplano, P. Tamarat, and B. Lounis, Tailoring the superradiant and subradiant nature of two coherently coupled quantum emitters, *Nature communications* **13**, 2962 (2022).
- [87] Z. Yan, J. Ho, Y.-H. Lu, S. J. Masson, A. Asenjo-Garcia, and D. M. Stamper-Kurn, Superradiant and subradiant cavity scattering by atom arrays, *Physical Review Letters* **131**, 253603 (2023).
- [88] T. E. Li, H.-T. Chen, A. Nitzan, and J. E. Subotnik, Quasiclassical modeling of cavity quantum electrodynamics, *Physical Review A* **101**, 033831 (2020).
- [89] T. Đorđević, P. Samutpraphoot, P. L. Ocola, H. Bernien, B. Grinkemeyer, I. Dimitrova, V. Vuletić, and M. D. Lukin, Entanglement transport and a nanophotonic interface for atoms in optical tweezers, *Science* **373**, 1511 (2021).
- [90] S. Ritter, C. Nölleke, C. Hahn, A. Reiserer, A. Neuzner, M. Uphoff, M. Mücke, E. Figueroa, J. Bochmann, and G. Rempe, An elementary quantum network of single atoms in optical cavities, *Nature* **484**, 195 (2012).
- [91] T. Tiecke, J. D. Thompson, N. P. de Leon, L. Liu, V. Vuletić, and M. D. Lukin, Nanophotonic quantum phase switch with a single atom, *Nature* **508**, 241 (2014).
- [92] T. Yoshie, A. Scherer, J. Hendrickson, G. Khitrova, H. Gibbs, G. Rupper, C. Ell, O. Shchekin, and D. Deppe, Vacuum Rabi splitting with a single quantum dot in a photonic crystal nanocavity, *Nature* **432**, 200 (2004).
- [93] A. M. Fox, *Quantum optics: an introduction*, Vol. 15 (Oxford University Press, USA, 2006).
- [94] Y. Liu, Z. Wang, P. Yang, Q. Wang, Q. Fan, S. Guan, G. Li, P. Zhang, and T. Zhang, Realization of strong coupling between deterministic single-atom arrays and a high-finesse miniature optical cavity, *Physical Review Letters* **130**, 173601 (2023).
- [95] Y. Han, H. Li, and W. Yi, Interaction-enhanced superradiance of a Rydberg-atom array, arXiv preprint arXiv:2405.01945 (2024).
- [96] S. Philipp, M. Göppl, J. Fink, M. Baur, R. Bianchetti, L. Steffen, and A. Wallraff, Multimode mediated qubit-qubit coupling and dark-state symmetries in circuit quantum electrodynamics, *Physical Review A* **83**, 063827 (2011).
- [97] D. Lentrodt, O. Diekmann, C. H. Keitel, S. Rotter, and J. Evers, Certifying multimode light-matter interaction in lossy resonators, *Physical Review Letters* **130**, 263602 (2023).
- [98] K. Yee, Numerical solution of initial boundary value problems involving Maxwell's equations in isotropic media, *IEEE Transactions on antennas and propagation* **14**, 302 (1966).
- [99] M. O. Scully and M. S. Zubairy, *Quantum optics* (Cambridge university press, 1997).
- [100] J. Oba, S. Kajita, and A. Soeda, Fast simulation for multi-photon, atomic-ensemble quantum model of linear optical systems addressing the curse of dimensionality, *Scientific Reports* **14**, 3208 (2024).

- [101] M. Havukainen, G. Drobny, S. Stenholm, and V. Bužek, Quantum simulations of optical systems, *journal of modern optics* **46**, 1343 (1999).
- [102] S. Bay, P. Lambropoulos, and K. Mølmer, Atom-atom interaction in strongly modified reservoirs, *Physical Review A* **55**, 1485 (1997).